Electronic Supplementary Information (ESI)

Superstructure-induced enhancement of solid-state triphenylacrylonitrile photochromism via a macrocycle-mediated blocking strategy

Meng-Hao Li,[a] Hui Hui,[a] Yan Wang,[a] and Ying-Wei Yang*[a]

[a] International Joint Research Laboratory of Nano-Micro Architecture Chemistry, College of Chemistry, Jilin University, 2699 Qianjin Street, Changchun 130012, P. R. China

E-mail: ywyang@jlu.edu.cn (Y.-W.Y.)

Table of Contents

Section 1. Instruments and methods

Solution ^{1}H and ^{13}C nuclear magnetic resonance (NMR) spectra were recorded on a Bruker Avance III 400 MHz NMR spectrometer, with TMS as the internal standard for chemical shift referencing. Mass spectrometry data were acquired using a Bruker Daltonics Autoflex Speed Series MALDI-TOF system and a Bruker Agilent 1290-micrOTOF Q II high-resolution (HR) mass spectrometer. Single-crystal X-ray diffraction data were collected on a Bruker D8 Venture diffractometer using ω-scans with graphite-monochromated Cu Kα radiation (λ = 1.54184 Å) and Mo Kα radiation (λ = 0.71073 Å). The diffraction experiment on the single crystals of TPAN-P5-CH_3OH was performed at the BL17B beamline, Shanghai Synchrotron Radiation Facility (SSRF). Powder X-ray diffraction patterns were obtained on a PANalytical B.V. Empyrean diffractometer, scanning from 5° to 30° (2θ) at a rate of 5° min-1. UV-Vis absorption spectra (liquid) were recorded on a Shimadzu UV-2550 spectrometer. A handheld 365 nm UV lamp was used: power, 5 W; irradiance, 50 and 90 mW/cm^2 at distances of 9 and 2 cm from the sample, respectively. These distances were used for liquid and solid samples, respectively. Under analogous conditions, illumination was performed using a handheld white-light flashlight with irradiances of 70 mW/cm^2 (distance: 9 cm) and 120 mW/cm^2 (distance: 2 cm). UV irradiance was measured using an LS125 UV radiometer (Shenzhen Linshang Technology Co., Ltd.). UV-Vis absorption spectra (solid) of the materials were obtained on a Perkin Elmer Lambda 950 spectrometer by measuring the diffuse reflectance of the powders. In-situ time-resolved solid-state UV-Vis absorption spectra were measured on a Shimadzu UV-3600i Plus, utilizing a 10 W radiation source at a distance of 20 cm. The scan range was 300-800 nm, with a medium scan rate. Photoluminescence (PL) spectra (solid), time-resolved fluorescence decay curves, and photoluminescence quantum yields were recorded using an Edinburgh FLS920 steady-state spectrometer. Quantum yields were calculated using an integrating sphere. PL spectra (solution) were measured using a Shimadzu RF-5301PC fluorescence spectrophotometer at room temperature. All photochromic films were compared to polymethyl methacrylate films, and the fatigue resistance of all films were tested by irradiating them under a 365 nm UV lamp to achieve maximum coloration, followed by irradiation with white light to induce bleaching until colorless. This process was repeated for five cycles. Single-crystal superstructure files were used as input for independent gradient model (IGM) analyses,[S1] which were carried out using Multiwfn 3.6 (function 20, visual study of weak interaction).[S2] The resulting data were visualized using Visual Molecular Dynamics (VMD) software.[S3] All calculations were based on the geometric structures determined from single-crystal X-ray diffraction. Frontier molecular orbitals were computed using density functional theory (DFT) at the B3LYP/6-31G(d,p) level, and natural transition orbitals (NTOs) were analyzed via time-dependent DFT (TDDFT) at the TD-B3LYP/6-31G(d,p) level. To ensure accuracy, Grimme's DFT-D3(BJ) dispersion correction was applied in all calculations. These computations were performed using the Gaussian 16 (Revision A.03) software package.[S4]

Section 2. Synthesis procedures

Unless otherwise stated, all reagents are purchased commercially and used without further purification.

2.1 Synthesis of TPAN-BO

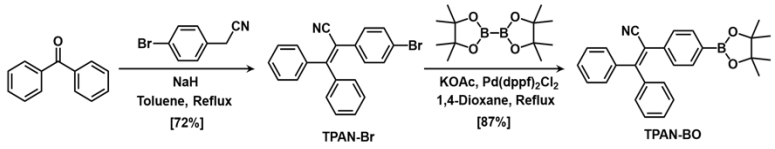

Scheme S1. Synthetic route of TPAN.

TPAN-Br and TPAN-BO were synthesized according to a published procedure.[S5]
TPAN-Br: ^{1}H NMR (400 MHz, $CDCl_3$, 298 K) δ 7.43 (d, *J* = 1.7 Hz, 5H), 7.35 (d, *J* = 8.6 Hz, 2H), 7.30 (d, *J* = 7.4 Hz, 1H), 7.22 (t, *J* = 7.4 Hz, 2H), 7.12 (d, *J* = 8.6 Hz, 2H), 7.00 (d, *J* = 7.0 Hz, 2H).
TPAN-BO: ^{1}H NMR (400 MHz, $CDCl_3$, 298 K) δ 7.64 (d, *J* = 7.7 Hz, 2H), 7.43 (d, *J* = 2.9 Hz, 5H), 7.27 (s, 1H), 7.25 – 7.21 (m, 2H), 7.21 – 7.14 (m, 2H), 6.99 (dd, *J* = 6.9, 1.8 Hz, 2H), 1.39 – 1.26 (m, 12H).

2.2 Synthesis of TPAN-P5

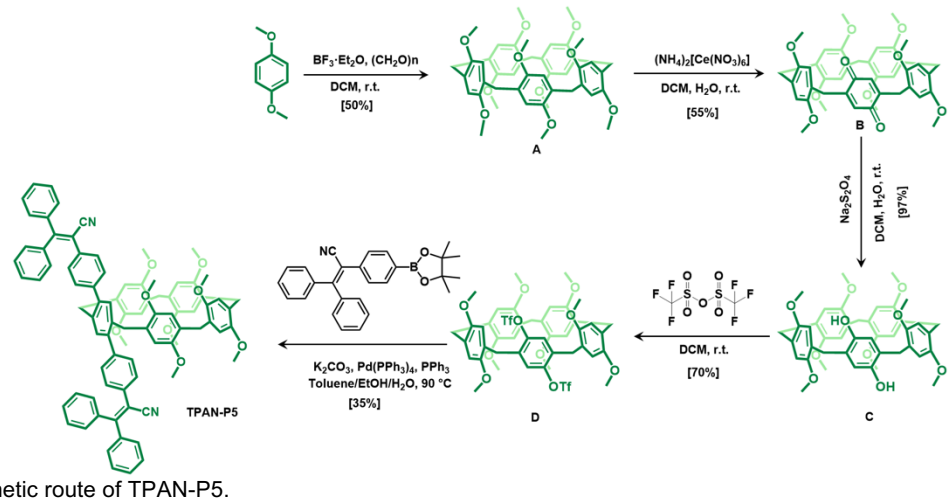

Scheme S2. Synthetic route of TPAN-P5.

The intermediate products A, B, C, and D used in the process were all synthesized according to the published methods.[S6]
A: ^{1}H NMR (400 MHz, $CDCl_3$, 298 K) δ (ppm) 6.76 (s, 10H), 3.77 (s, 10H), 3.64 (s, 30H).
B: ^{1}H NMR (400 MHz, $CDCl_3$, 298 K) δ (ppm) 6.85 (s, 2H), 6.82 (s, 2H), 6.80 (s, 2H), 6.68 (d, *J* = 3.4 Hz, 4H), 3.80 (s, 6H), 3.76 (s, 6H), 3.73 (s, 12H), 3.64 (s, 6H), 3.61 (s, 4H).
C: ^{1}H NMR (400 MHz, DMSO-d_6, 298 K) δ (ppm) 8.21 (s, 2H), 6.90 – 6.73 (m, 8H), 6.55 (s, 2H), 3.73 – 3.51 (m, 34H).
D: ^{1}H NMR (400 MHz, $CDCl_3$, 298 K) δ (ppm) δ 7.35 (s, 2H), 6.81 (s, 2H), 6.79 (s, 2H), 6.77 (s, 2H), 6.70 (s, 2H), 3.85 (s, 3H), 3.79 (s, 6H), 3.73 (s, 6H), 3.69 (s, 6H), 3.67 (s, 6H), 3.62 (s, 6H).
TPAN-P5: Compound D (400 mg, 0.4 mmol), TPAN-BO (488 mg, 0.6 mmol), $Pd(PPh_3)_4$ (23 mg, 0.02 mmol), and K_2CO_3 (1.4 g, 10 mmol) were sequentially added to a 50 mL thick-walled pressure vessel. Under a nitrogen atmosphere (glove box), a mixture of toluene/ethanol/water (v/v/v, 12:4:4) was added. The reaction vessel was heated at 90 °C for 48 hours. The reaction mixture was then extracted three times with ethyl acetate (EA) and saturated aqueous NaCl solution. The organic phases were collected, and the solvent was removed under reduced pressure to afford a crude product. Purification by silica gel column chromatography yielded a white powder, which transformed into a pale yellow powder after drying and activation to remove solvent from the cavities (eluent: dichloromethane (DCM)/petroleum ether (PE) = 1:10; yield: 175 mg, 35%). Mp: 149.2-151.3 °C. ^{1}H NMR (400 MHz, $CDCl_3$, 298 K) δ 7.47 (p, *J* = 3.7 Hz, 10H), 7.29 (d, *J* = 7.4 Hz, 3H), 7.25 – 7.19 (m, 7H), 7.14 (s, 2H), 7.10 – 7.04 (m, 4H), 7.01 (d, *J* = 8.2 Hz, 4H), 6.76 (s, 2H), 6.70 (s, 2H), 6.57 (s, 2H), 5.84 (s, 2H), 3.81 (s, 6H), 3.74 (d, *J* = 3.5 Hz, 4H), 3.64 (s, 6H), 3.56 (s, 6H), 3.44 (s, 6H), 3.37 (s, 6H). ^{13}C NMR (126 MHz, $CDCl_3$, 298 K) δ 157.77, 150.95, 150.60, 142.54, 140.38, 139.60, 139.13, 136.23, 133.15, 132.55, 130.83, 130.03, 129.96, 129.68, 129.33, 129.12, 128.74, 128.54, 128.33, 128.11, 127.68, 120.18, 114.43, 113.90, 113.76, 113.71, 111.21, 56.06, 55.87, 55.84, 55.35, 32.54, 29.99. HRMS (m/z): $C_{85}H_{72}N_2O_8$ calcd. $[M+Na]^+$ 1271.5180, found 1271.5003.

2.3 Synthesis of TPAN-Ph

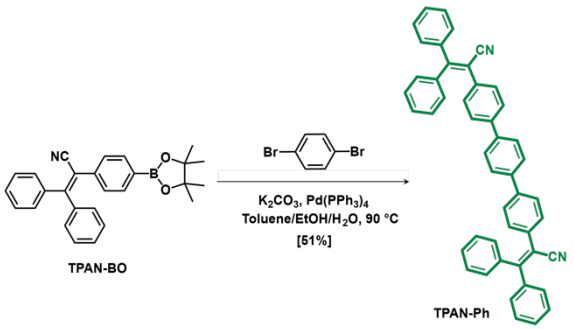

Scheme S3. Synthetic route of TPAN-Ph.

p-Dibromobenzene (354 mg, 1.5 mmol), TPAN-BO (1.8 g, 4.5 mmol), $Pd(PPh_3)_4$ (87 mg, 0.075 mmol), and K_2CO_3 (1.7 g, 12 mmol) were sequentially added to a 50 mL thick-walled pressure tube. A mixture of toluene/ethanol/water (v/v/v = 15:5:5) was then added under a N_2 atmosphere. After reacting at 90 °C for 48 hours, the work-up procedure was the same as that for TPAN-P5, involving extraction and purification by silica gel column chromatography to afford a white powder (eluent: DCM/PE/EA = 2:4:1; yield: 487 mg, 51%). Mp: 291.8-293.2 °C. ^{1}H NMR (500 MHz, $CDCl_3$, 298 K) δ 7.63 (s, 4H), 7.53 – 7.41 (m, 14H), 7.35 (d, *J* = 8.4 Hz, 4H), 7.29 (t, *J* = 7.3 Hz, 2H), 7.23 (t, *J* = 7.4 Hz, 4H), 7.11 – 7.03 (m, 4H). ^{13}C NMR (126 MHz, $CDCl_3$, 298 K) δ 157.74, 140.44, 140.21, 139.12, 133.91, 130.80, 130.20, 129.97, 129.95, 129.10, 128.47, 128.37, 127.36, 126.86, 120.12, 111.15. MALDI-TOF: $C_{48}H_{32}N_2$ calcd. $[M]^+$ m/z 636.2638, found $[M]^+$ m/z 636.2202.

2.4 Preparation of poly(methyl methacrylate) (PMMA) films with varying TPAN-P5 loadings

To prepare the solutions, TPAN-P5 powder was mixed with a quantity of PMMA (100 mg) at concentrations of 0.5, 1.0, 1.5, and 2 wt.% ($m_{TPAN-P5}$: m_{PMMA}). The resulting mixture was then transferred to a 5 mL glass vial, and 1.5 mL of $CHCl_3$ was added until complete dissolution. Glass slides measuring 18 mm × 18 mm were selected as film substrates. Subsequently, 162 μL (0.5 μL/mm^2) and 227 μL (0.7 μL/mm^2) a aliquots of the prepared solution were uniformly drop-cast onto the glass slides. After allowing the $CHCl_3$ to slowly evaporate, films with corresponding concentrations and thicknesses were obtained.

Section 3. NMR and mass spectroscopy

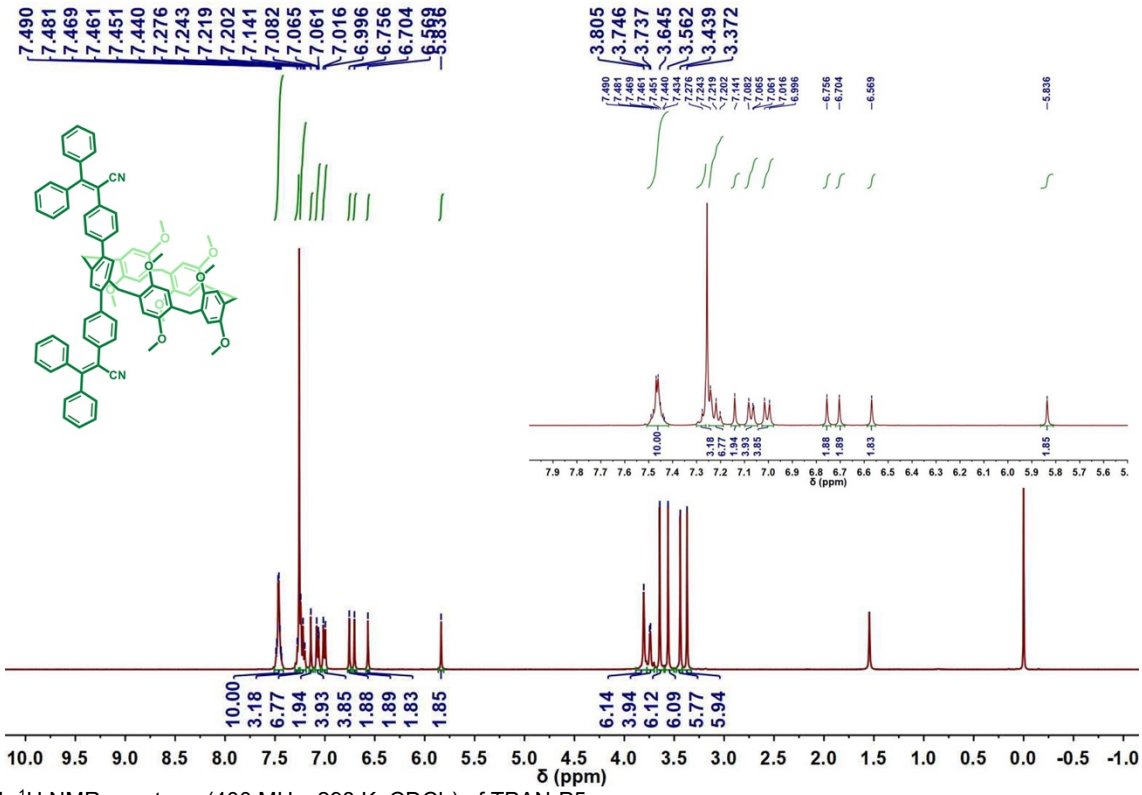

Figure S1. ^{1}H NMR spectrum (400 MHz, 298 K, $CDCl_3$) of TPAN-P5.

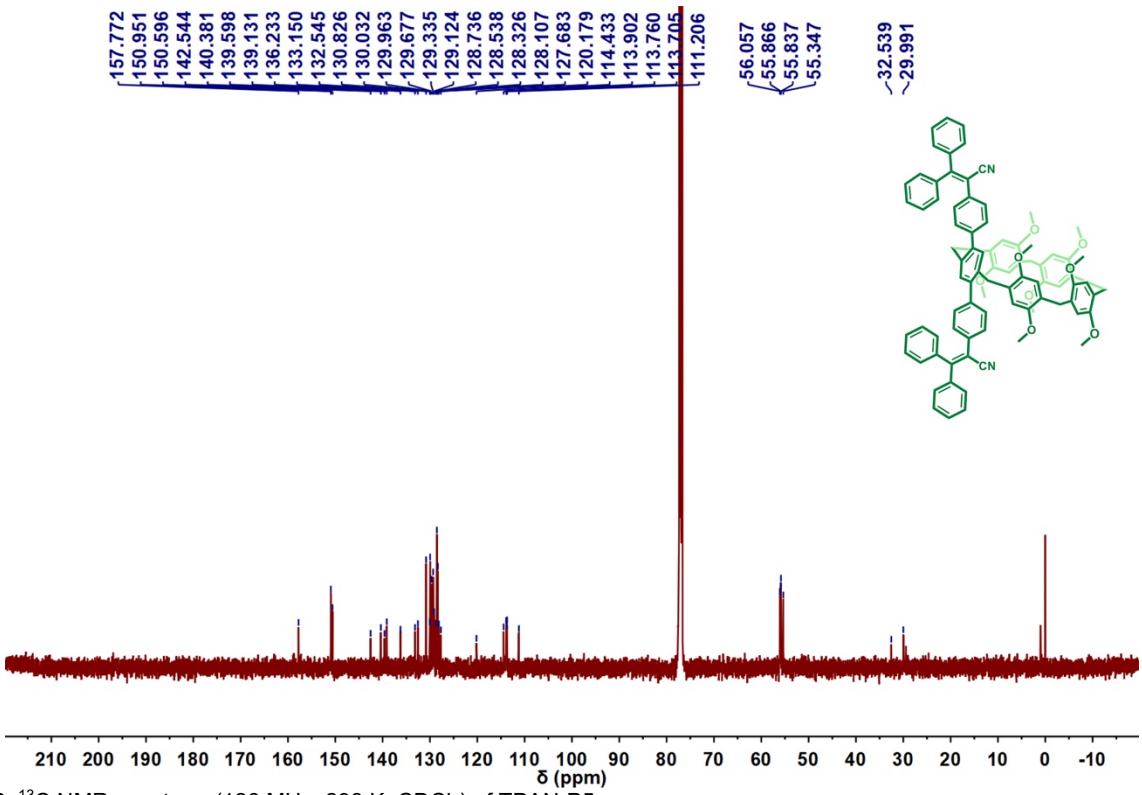

Figure S2. ^{13}C NMR spectrum (126 MHz, 298 K, $CDCl_3$) of TPAN-P5.

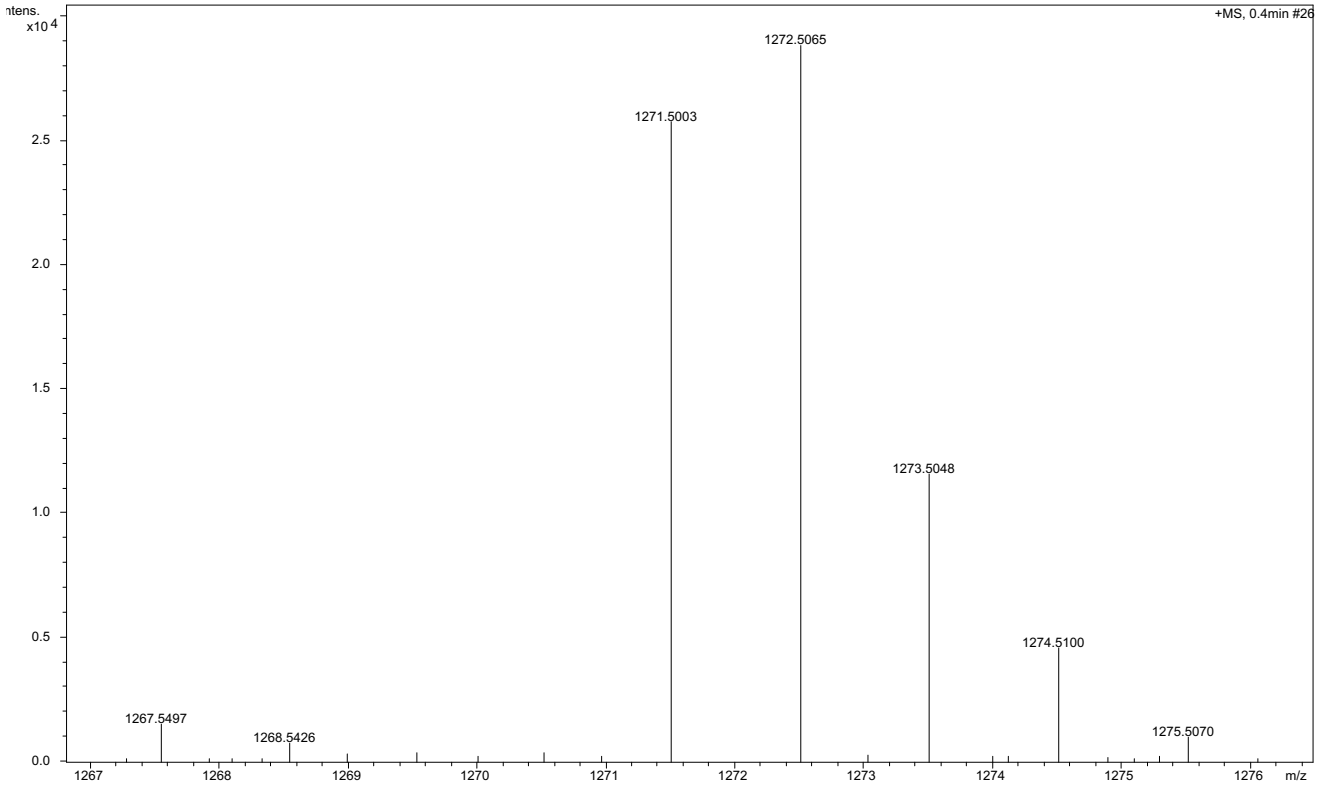

Figure S3. HRMS spectrum of TPAN-P5.

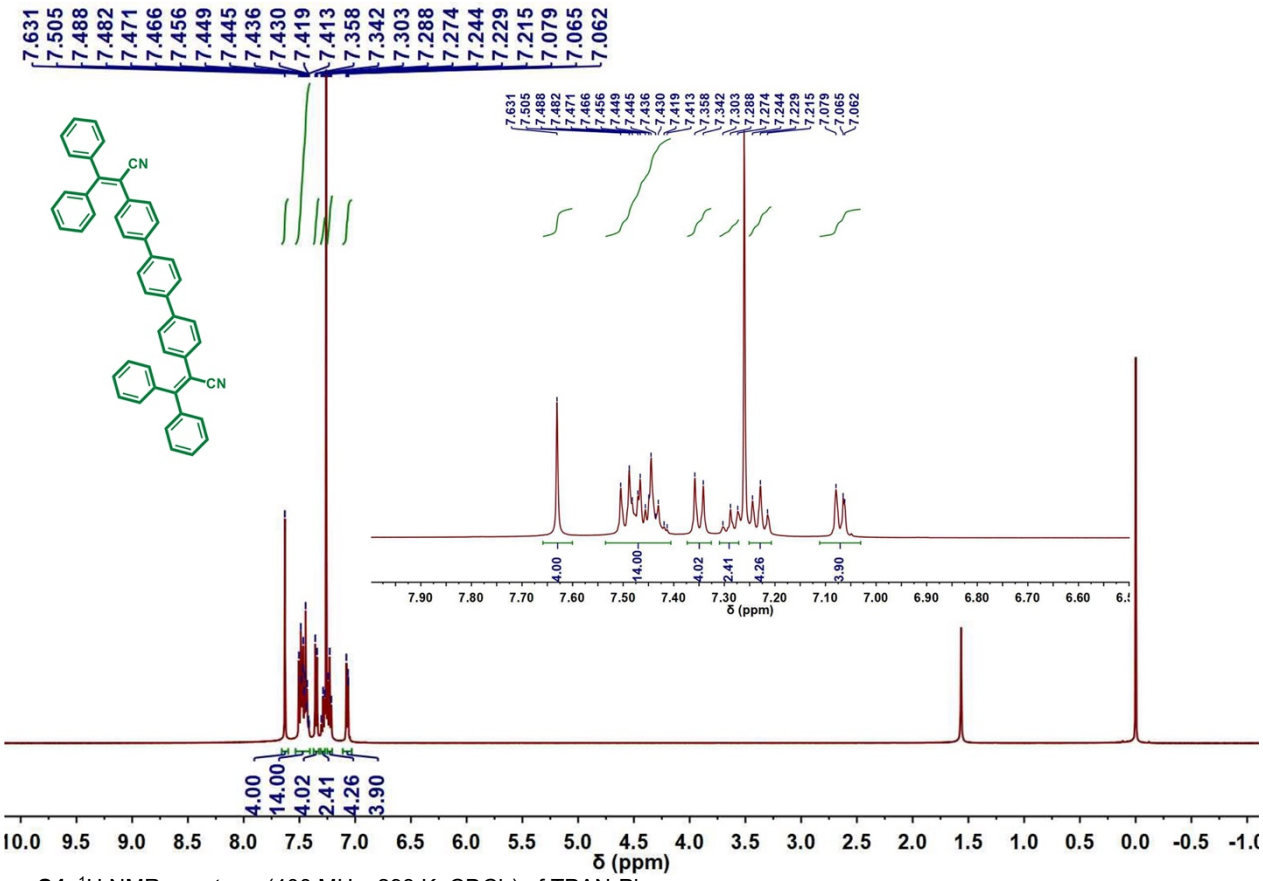

Figure S4. ^{1}H NMR spectrum (400 MHz, 298 K, $CDCl_3$) of TPAN-Ph.

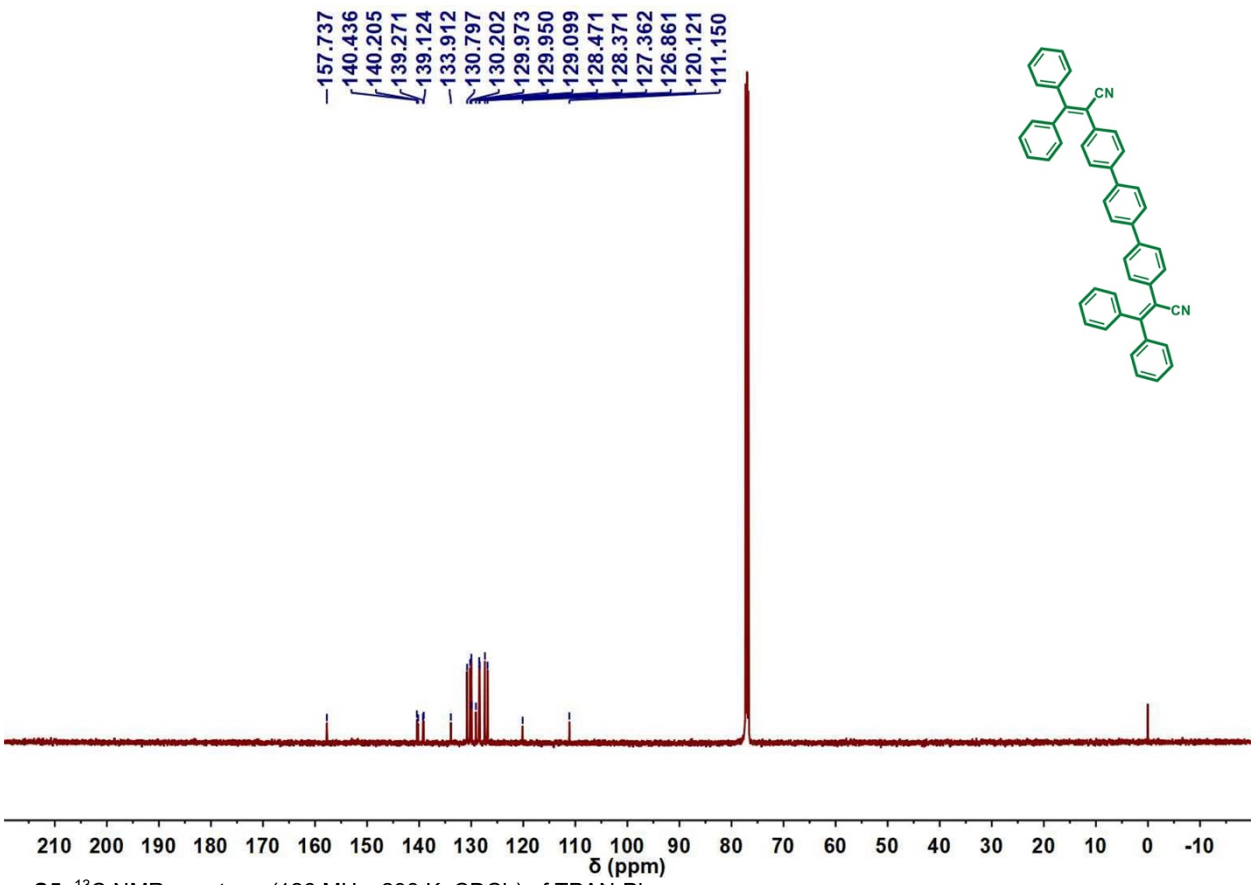

Figure S5. ^{13}C NMR spectrum (126 MHz, 298 K, $CDCl_3$) of TPAN-Ph.

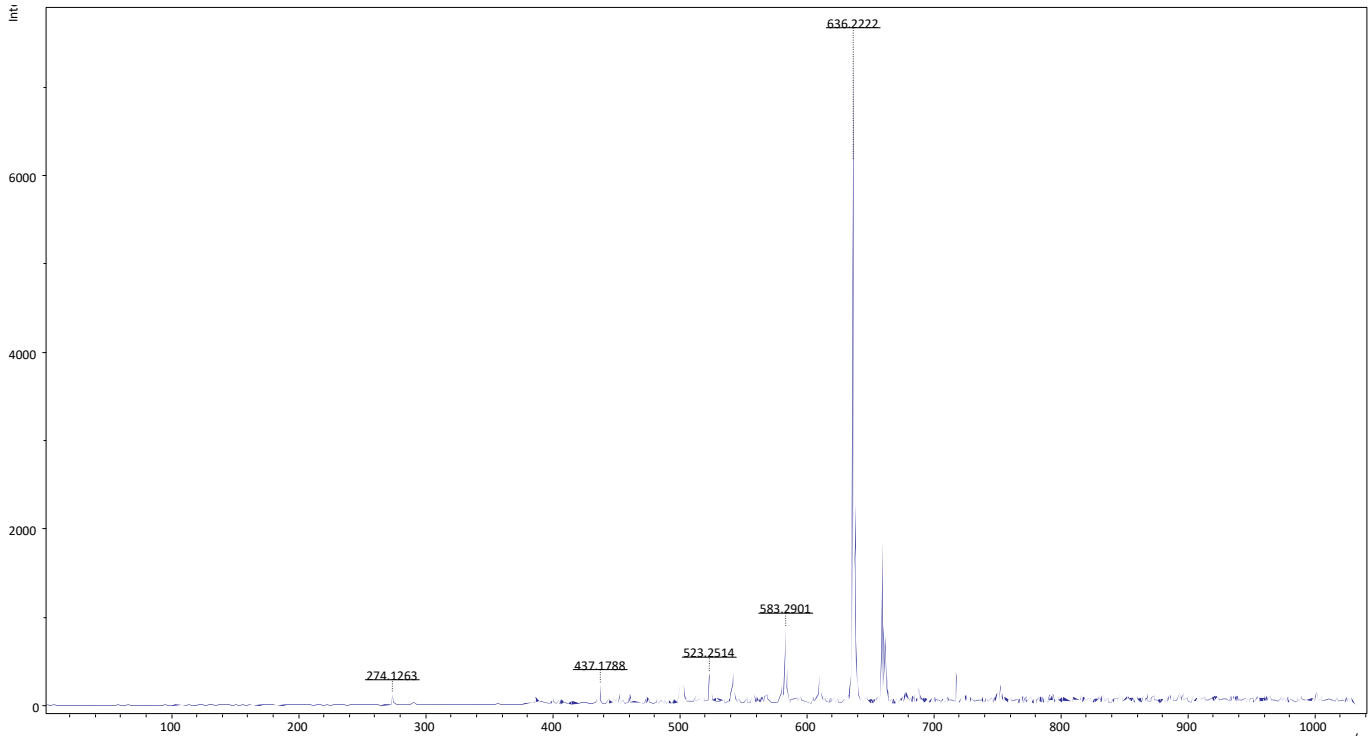

Figure S6. MALDI-TOF-MS spectrum of TPAN-Ph.

Section 4. Crystal structure analysis

TPAN-P5: TPAN-P5 powder (2 mg) was dissolved in 1 mL of a mixture of CH_3OH and CH_2Cl_2 (v/v = 0.2:0.8). Colorless block crystals, suitable for X-ray diffraction, formed after 48 hours of solvent evaporation.
TPAN-Ph: To obtain crystals suitable for X-ray diffraction, 2 mg of TPAN-P5 powder was dissolved in 1 mL of a mixture of CH_3OH and $CHCl_3$ (v/v = 0.5:0.5). After 48 hours of slow solvent evaporation, colorless block crystals formed.
TPAN-P5-CH_3OH: Colorless block single crystals of the methanol solvate TPAN-P5-CH_3OH, suitable for X-ray diffraction, were grown by slow evaporation over 72 hours from a solution containing 2 mg of TPAN-P5 in 1 mL of CH_3OH/CH_2Cl_2 (0.6:0.4 v/v).
TPAN-P5-EA: Colorless block single crystals of TPAN-P5-EA suitable for X-ray diffraction were obtained by dissolving 2 mg of the powder in 1 mL of CH_3OH/EA (0.2:0.8 v/v) and allowing the solvent to evaporate over 72 hours.
TPAN-P5-CH_3CH_2OH: Colorless spindle-shaped crystals were prepared by dissolving 2 mg of TPAN-P5 in 1 mL of a CH_2Cl_2/CH_3CH_2OH mixture (0.8:0.2 v/v) and allowing the solvent to evaporate over 48 hours.
TPAN-P5-CH_3COOH: Colorless spindle-shaped crystals were obtained by the slow evaporation of a 1 mL mixed solvent (CH_2Cl_2/CH_3COOH, 0.8:0.2 v/v) containing 2 mg of TPAN-P5 for 96 hours.

Table S1. Single crystal data

Compound	**TPAN-P5+solvent**	**TPAN-Ph+$CHCl_3$**
Empirical formula	$C_{85}H_{72}N_2O_8$	$C_{49}H_{33}Cl_3N_2$
Formula weight	1249.44	756
Crystal system	monoclinic	monoclinic
Space group	P2/n	$P2_1/c$
a/Å	15.5235(15)	9.24260(10)
b/Å	12.3965(10)	43.0831(5)
c/Å	20.4377(15)	19.3643(2)
a/deg	90	90
b/deg.	102.146(6)	93.2900(10)
γ/deg	90	90
V/Å^3	3844.9(6)	7698.15(15)
Z	2	8
ρ_{calcg}/cm^3	1.079	1.305
μ/mm $^{-1}$	0.069	2.441
F(000)	1320.0	3136.0
Theta range/deg.	5.48 to 49.996	4.102 to 153.324
Reflections collected	81299	90139
R(int)	0.0684	15942
R_1, wR_2 [obs I > 2σ (I)]	0.1004, 0.1950	0.0756, 0.1621
R_1, wR_2 (all data)	0.1153, 0.2042	0.0853, 0.1655
CCDC number	2379605	2379600

Note: Due to solvent disorder in TPAN-P5, the solvent contribution was removed from the analysis.

Table S2. Single crystal data

Compound	**TPAN-P5-CH_3OH**	**TPAN-P5-EA**	**TPAN-P5-CH_3CH_2OH**	**TPAN-P5-CH_3COOH**
Empirical formula	$C_{88.5}H_{84}Cl_2N_2O_{10.5}$	$C_{93}H_{88}N_2O_{12}$	$C_{90}H_{86}Cl_2N_2O_{10}$	$C_{90}H_{82}Cl_2N_2O_{12}$
Formula weight	1414.47	1425.65	1426.5	1454.47
Crystal system	monoclinic	monoclinic	monoclinic	monoclinic
Space group	C2/c	$P2_1/n$	C2/c	C2/c
a/Å	31.0098(10)	17.7269(8)	45.8525(9)	45.8868(17)
b/Å	24.3849(8)	22.0508(11)	13.1186(3)	13.1150(5)
c/Å	22.9318(7)	20.6123(11)	33.5659(7)	33.8049(13)
a/deg	90	90	90	90
b/deg.	120.0240(10)	103.142(2)	132.1990(10)	132.234(2)
γ/deg	90	90	90	90
V/$Å^3$	15013.5(8)	7846.2(7)	14957.5(6)	15062.8(10)
Z	8	4	8	8
ρ_{calcg}/cm^3	1.252	1.207	1.267	1.283
μ/mm^{-1}	0.150	0.079	1.284	1.308
F(000)	5976.0	3024.0	6032.0	6128.0
Theta range/deg.	2.186 to 49.73	5.052 to 50.164	5.28 to 127.49	5.202 to 137.406
Reflections collected	73123	204316	63013	89425
R(int)	0.0772	0.0467	0.0271	0.0817
R_1, wR_2 [obs I > 2σ (I)]	0.1240, 0.3586	0.0623, 0.1503	0.0778, 0.2279	0.0687, 0.1962
R_1, wR_2 (all data)	0.1315, 0.3737	0.0862, 0.1753	0.0815, 0.2316	0.0917, 0.2218
CCDC number	2448876	2380579	2488767	2488768

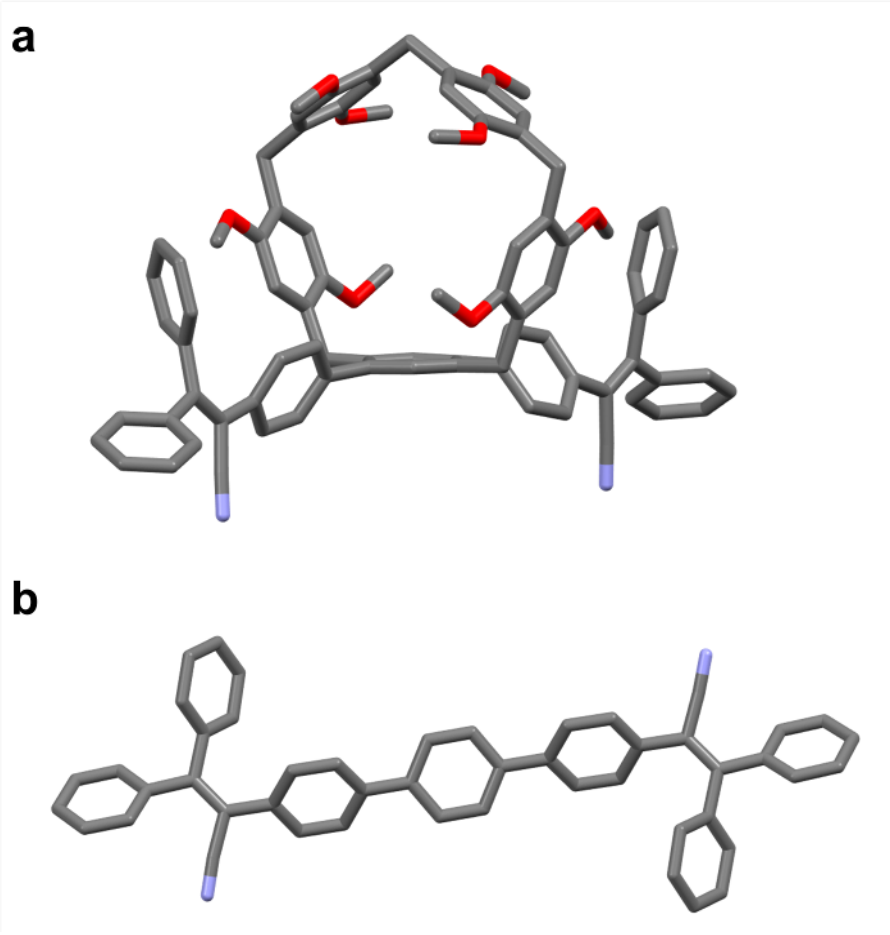

Figure S7. Crystal structures of TPAN-P5 (a) and TPAN-Ph (b).

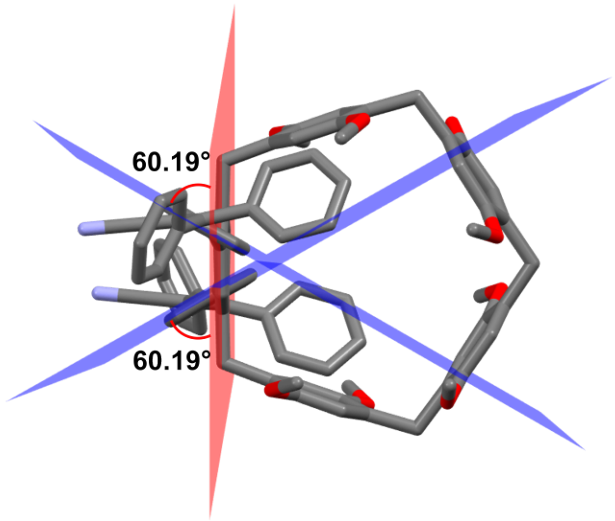

Figure S8. Dihedral angles between terphenyl units in TPAN-P5. Dihedral angles are measured between the terphenyl units with respect to the pillar[5]arene plane in the TPAN-P5 crystal structure.

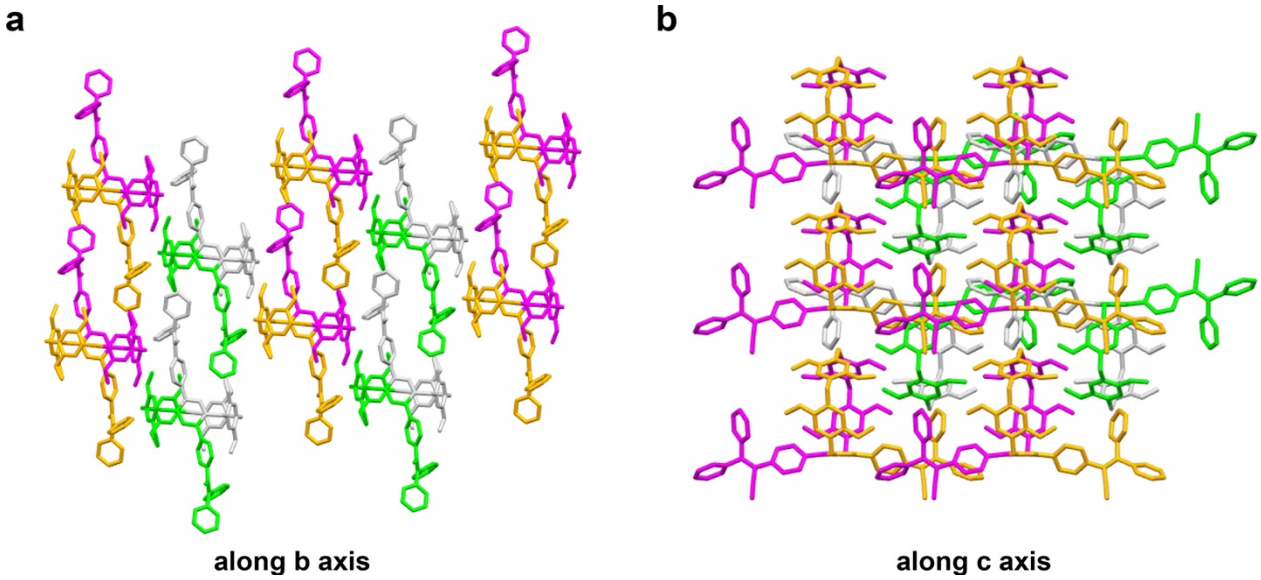

Figure S9. Crystal structure and packing of TPAN-P5 viewed along the b (a) and c (b) axes. Hydrogen atoms are omitted for clarity.

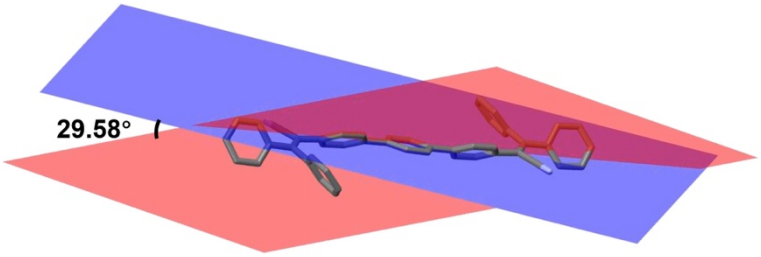

Figure S10. Dihedral angles between terphenyl units in TPAN-Ph. Hydrogen atoms are omitted for clarity.

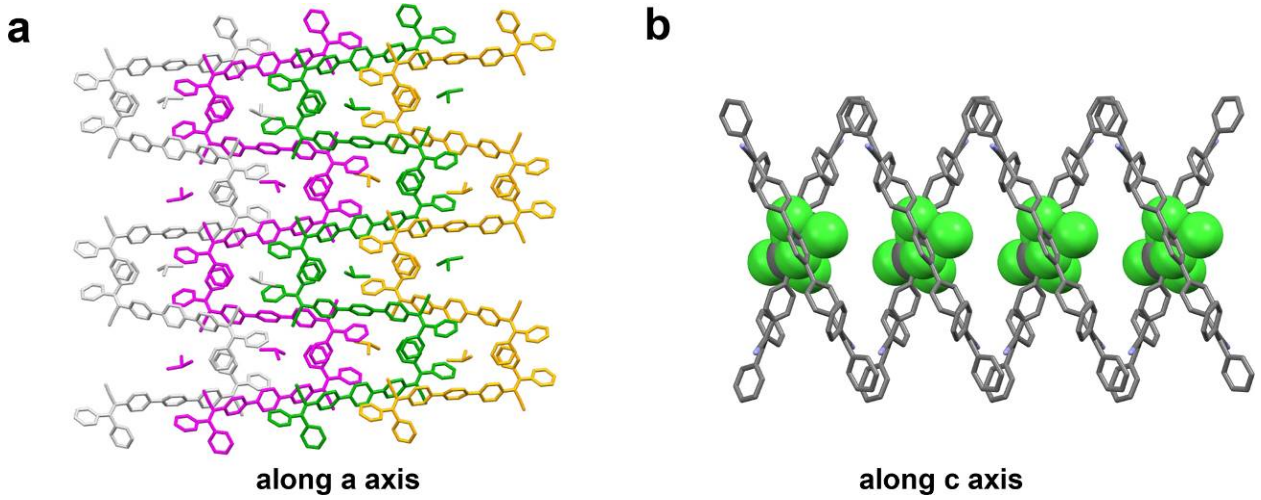

Figure S11. Crystal structure and packing of TPAN-Ph viewed along the a (a) and c (b) axes. Hydrogen atoms are omitted for clarity. The solvent contained in the crystals is $CHCl_3$.

Section 5. Characterization and photoresponsive properties

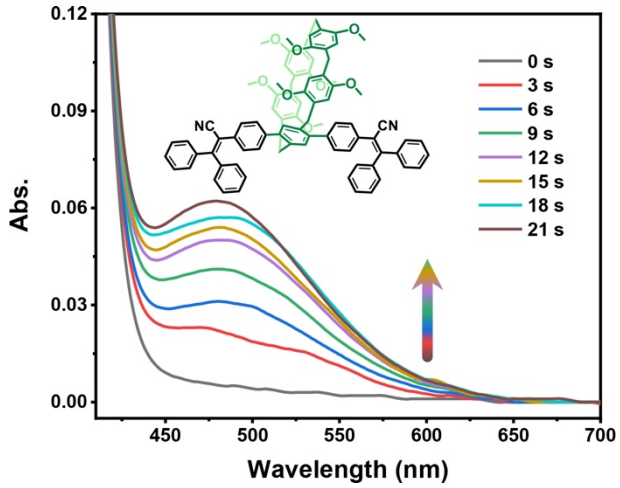

Figure S12. Transient UV-Vis absorption spectra of TPAN-P5 in CH_2Cl_2 (c = 10^{-3} M) under 365 nm UV irradiation for different times.

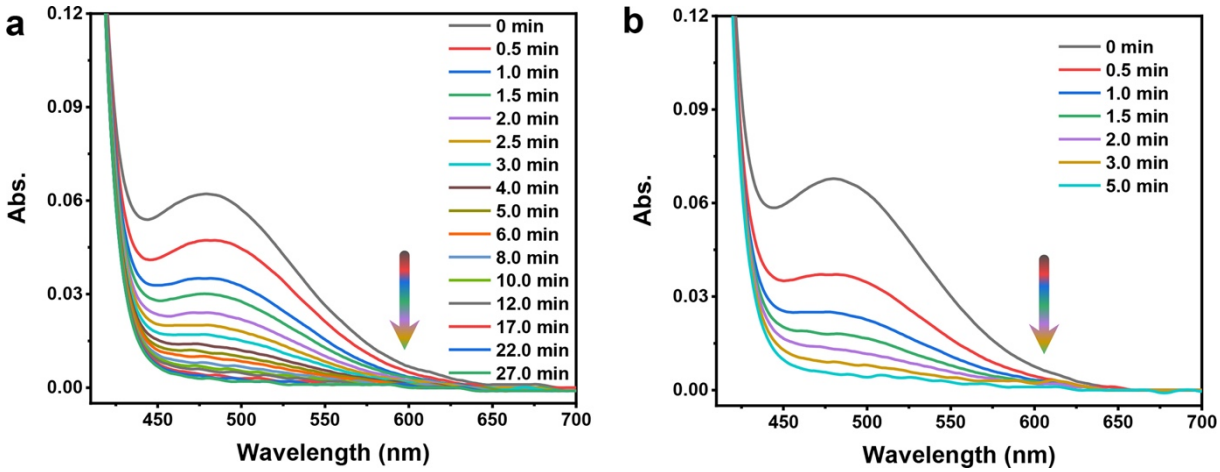

Figure S13. Transient UV-Vis absorption spectra of TPAN-P5 in CH_2Cl_2 (c = 10^{-3} M) in darkness (a) and under white light (b).

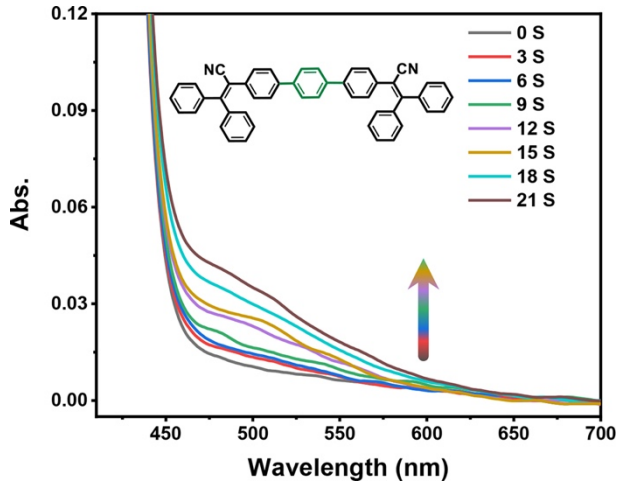

Figure S14. Transient UV-Vis absorption spectra of TPAN-Ph in CH_2Cl_2 (c = 10^{-3} M) under 365 nm UV irradiation for different times.

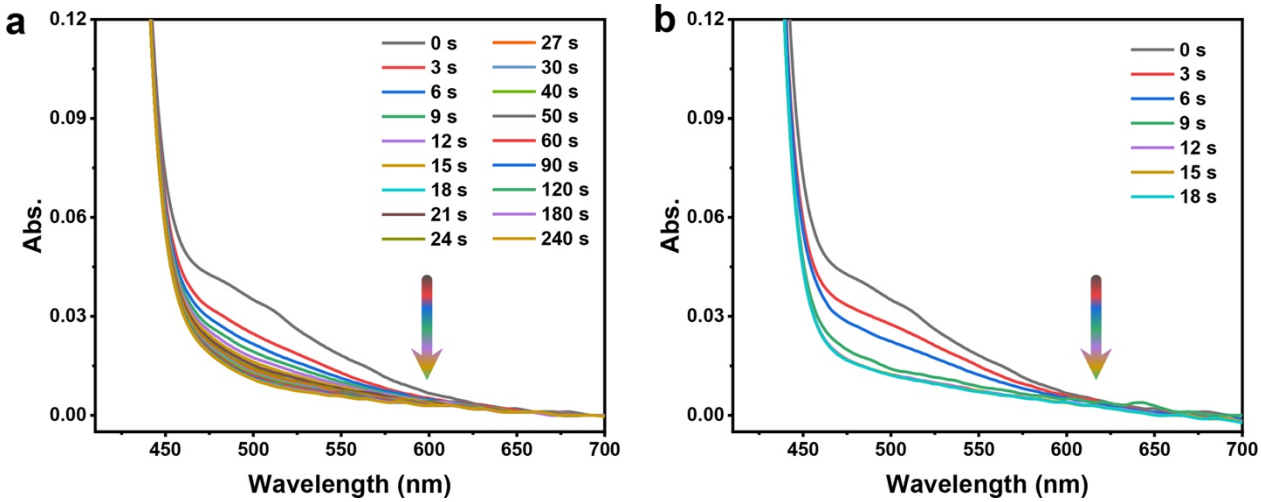

Figure S15. Transient UV-Vis absorption spectra of TPAN-Ph in CH_2Cl_2 (c = 10^{-3} M) in darkness (a) and under white light (b).

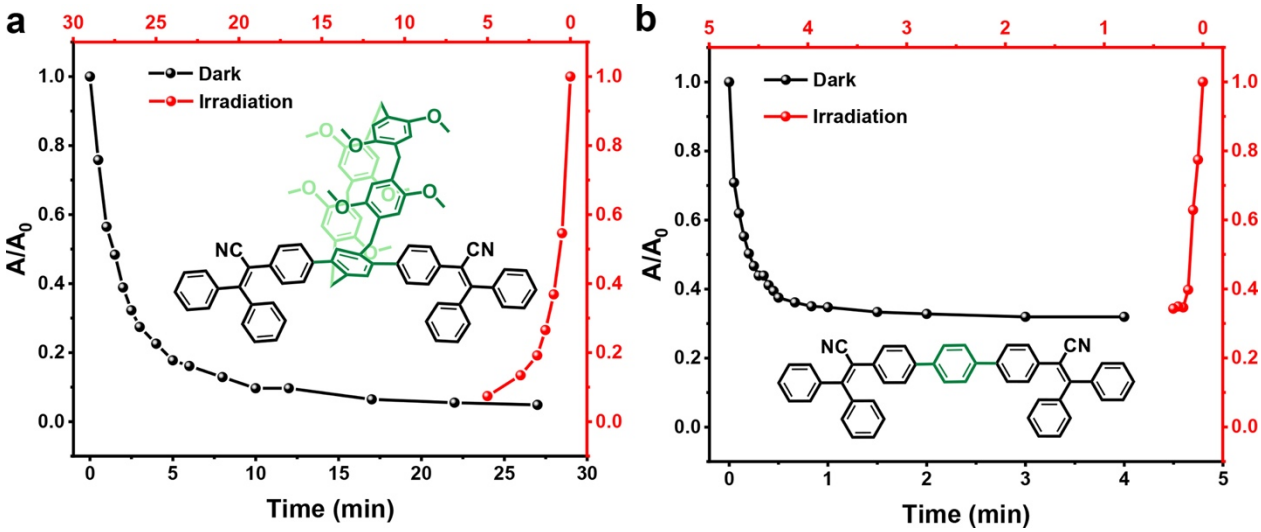

Figure S16. Time-dependent light bleaching curves of TPAN-P5 (a) and TPAN-Ph (b) in CH_2Cl_2 (c = 10^{-3} M) in the dark and under white light after removal of UV irradiation.

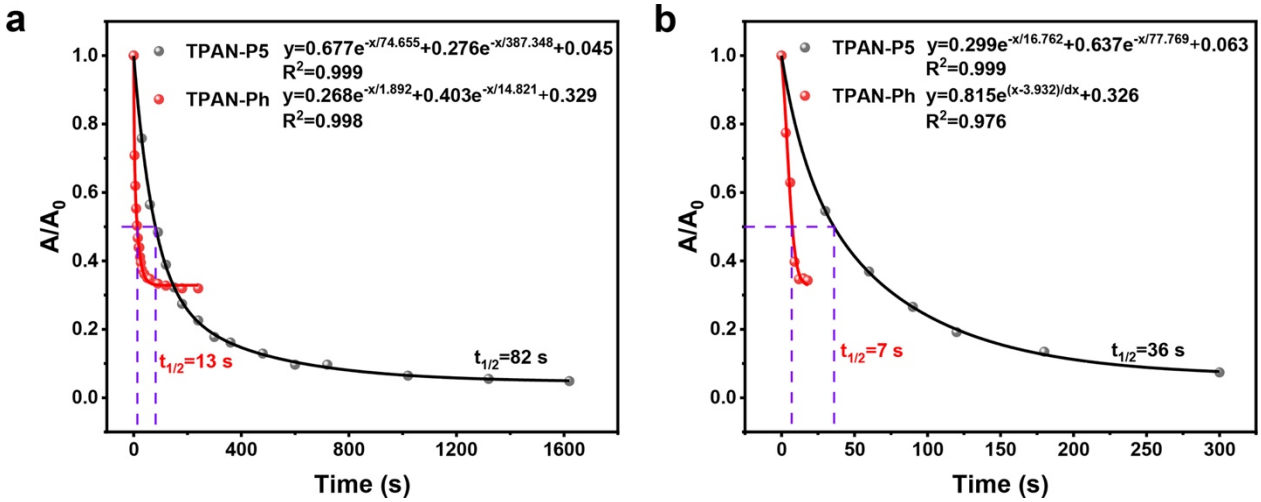

Figure S17. Time-dependent bleaching fitting curves of UV-irradiated TPAN-P5 and TPAN-Ph in CH_2Cl_2 (c = 10^{-3} M), measured in the dark (a) and under white light (b).

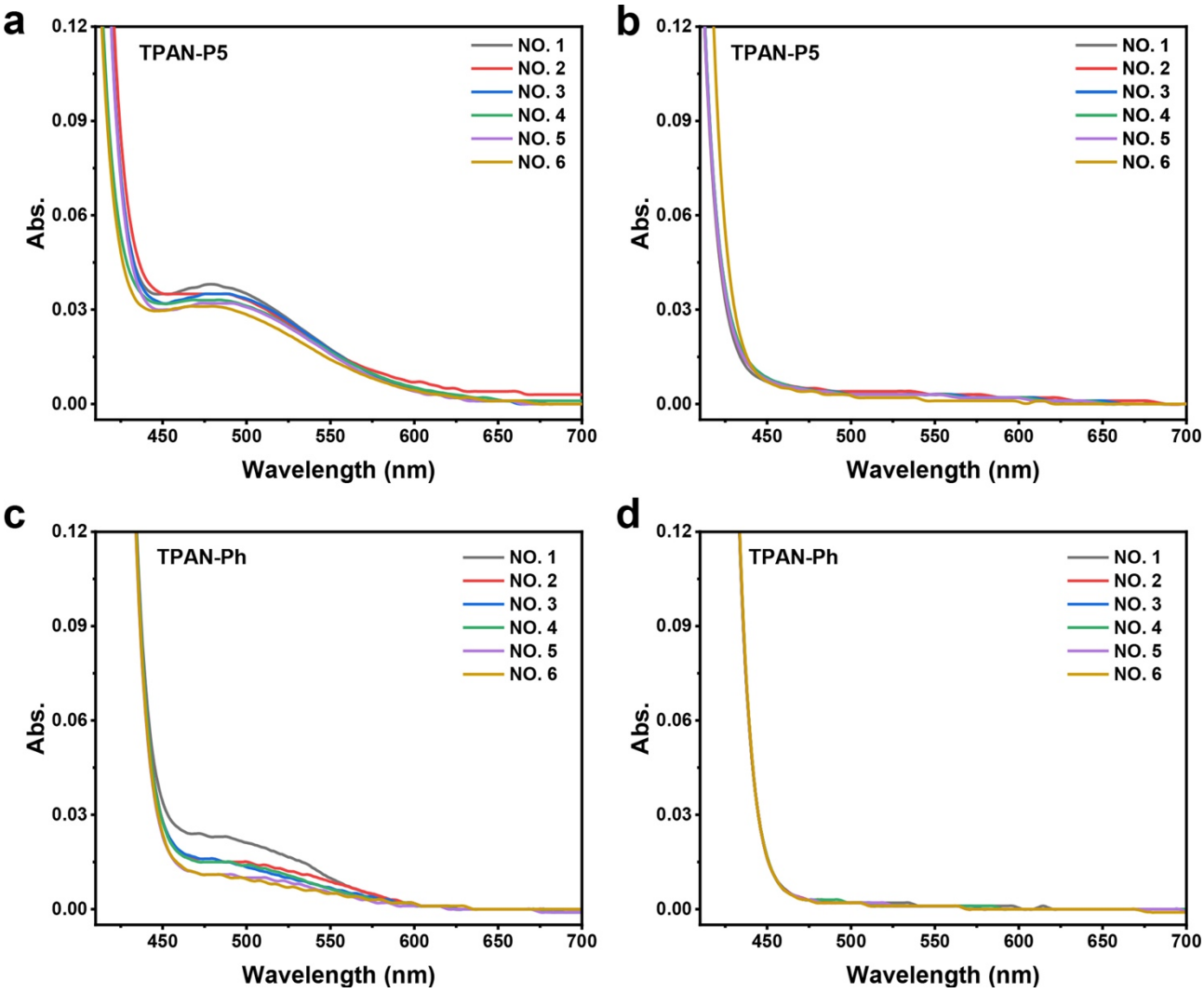

Figure S18. Cyclic stability/Fatigue resistance of TPAN-P5 and TPAN-Ph in CH_2Cl_2 (c = 10^{-3} M) under alternating UV/Vis irradiation.

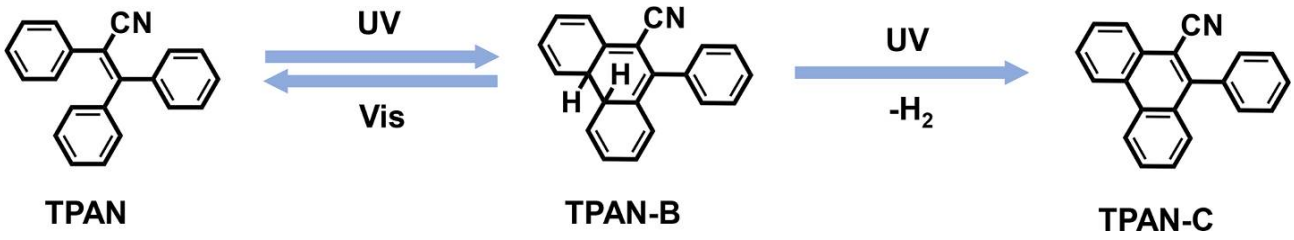

Figure S19. Structural evolution of TPAN during photoirradiation reaction.

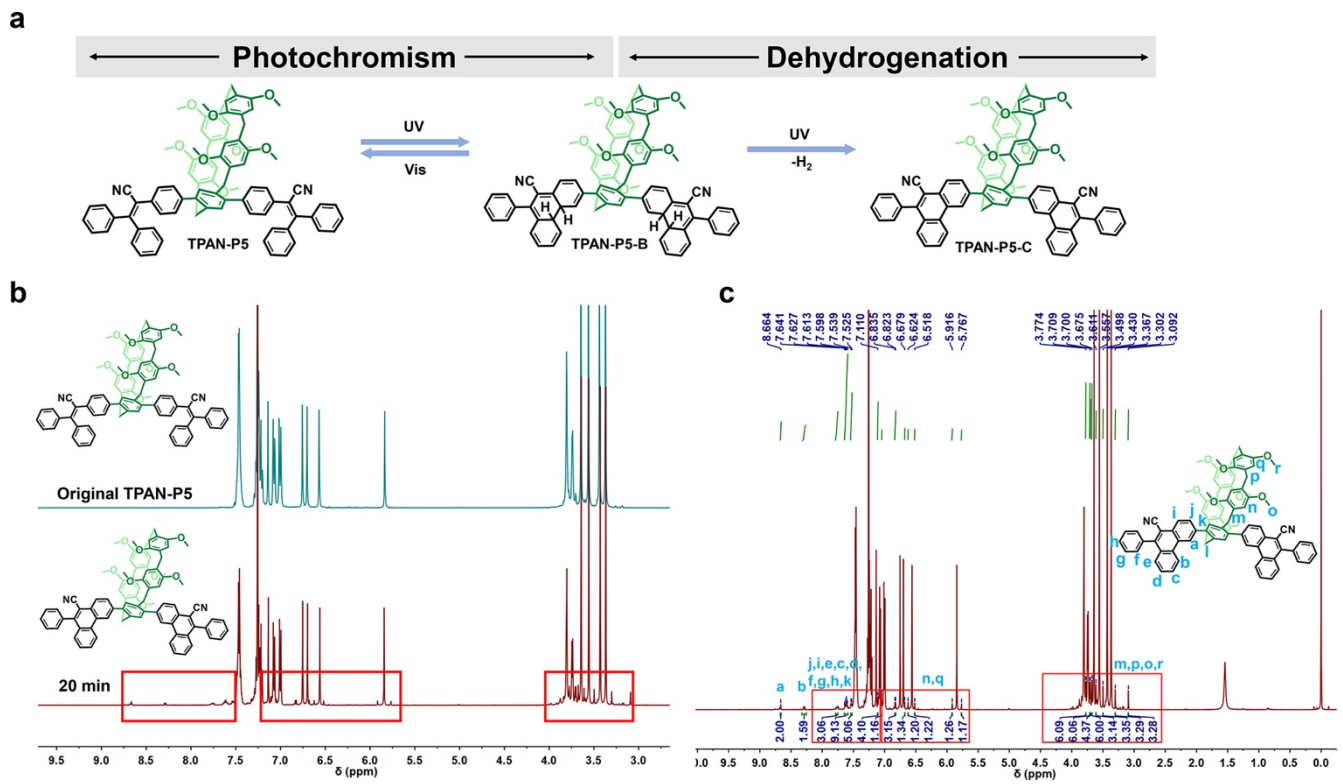

Figure S20. (a) Structural evolution of TPAN-P5 during photoirradiation reaction. (b and c) ^{1}H NMR spectra of TPAN-P5 before and after UV irradiation (400 MHz, 298 K, $CDCl_3$).

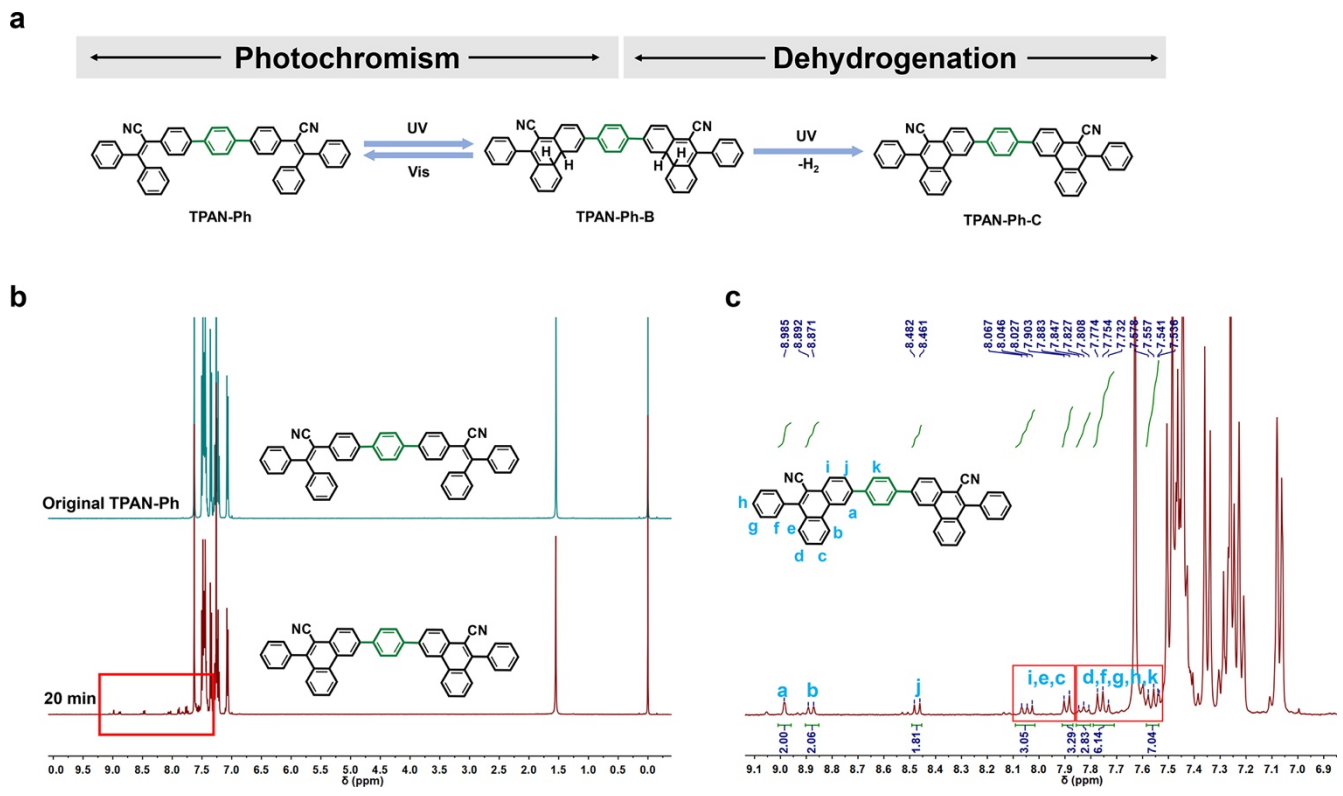

Figure S21. (a) Structural evolution of TPAN-Ph during photoirradiation reaction. (b and c) ^{1}H NMR spectra of TPAN-Ph before and after UV irradiation (400 MHz, 298 K, $CDCl_3$).

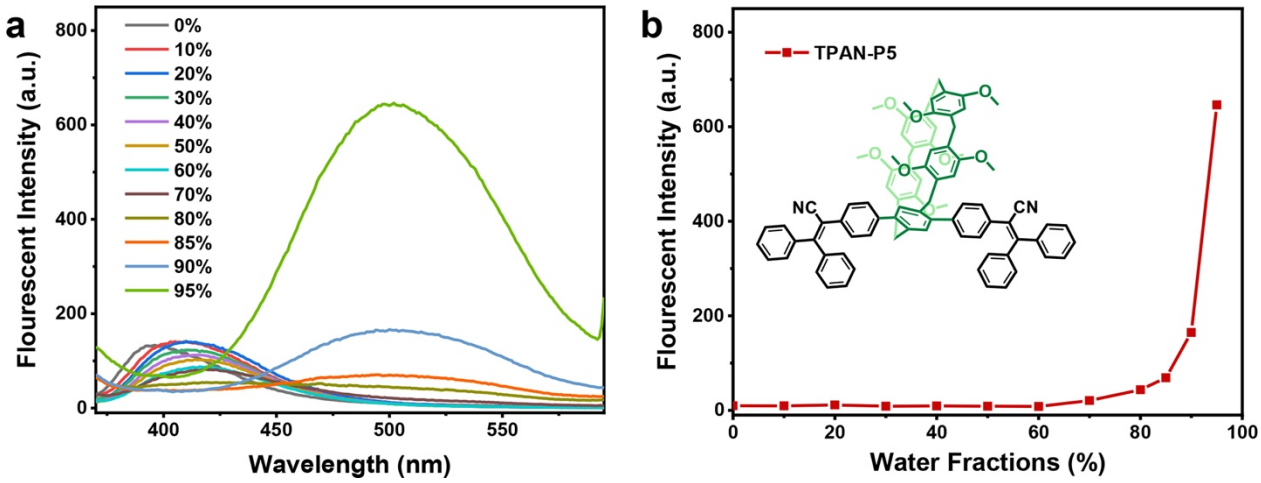

Figure S22. (a) PL spectra of dilute solutions (c = 10^{-5} M) of TPAN-P5 in H_2O/THF mixtures containing different H_2O fractions (f_w). (b) Plots of the emission intensity versus f_w of TPAN-P5.

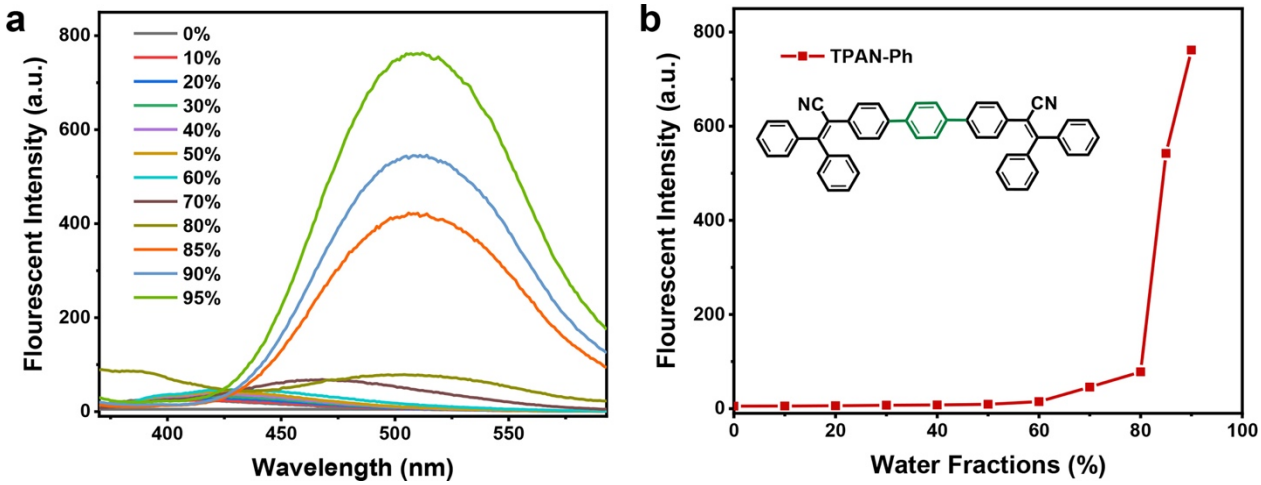

Figure S23. (a) PL spectra of dilute solutions (c = 10^{-5} M) of TPAN-Ph in H_2O/THF mixtures containing different H_2O fractions (f_w). (b) Plots of the emission intensity versus f_w of TPAN-Ph.

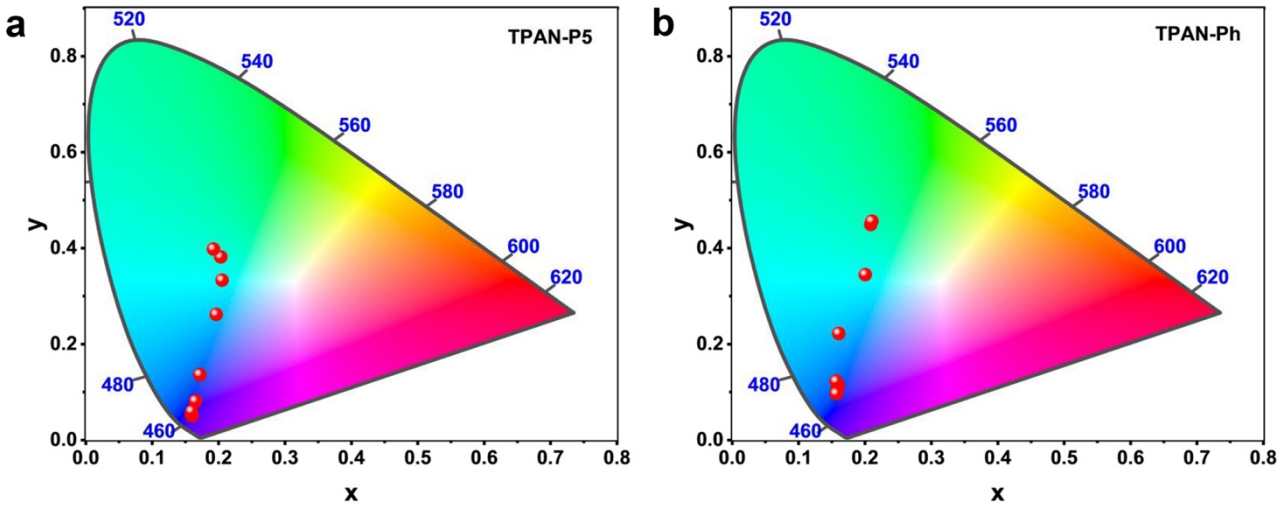

Figure S24. Fluorescence CIE diagrams of TPAN-P5 (a) and TPAN-Ph (b) in solutions with different aggregation states.

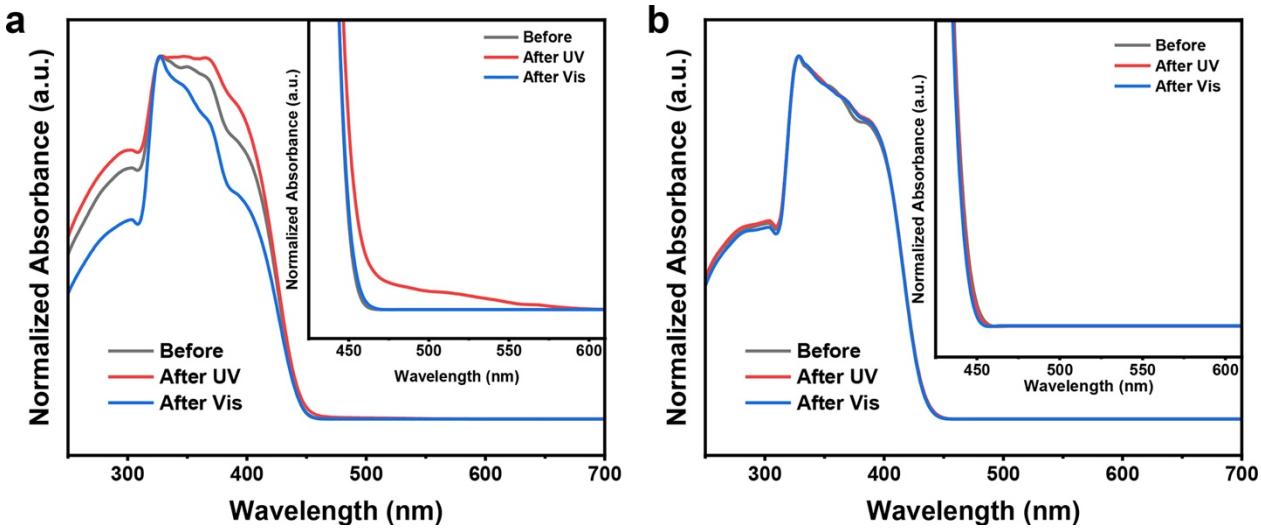

Figure S25. Normalized solid-state UV-Vis absorption spectra of TPAN-P5 (a) and TPAN-Ph (b) powders at different light irradiation conditions, initial (black line), UV-irradiated (blue line, 1 minutes), and white light-irradiated (red line, 2 minutes). Inset: Expanded UV-Vis absorption spectra.

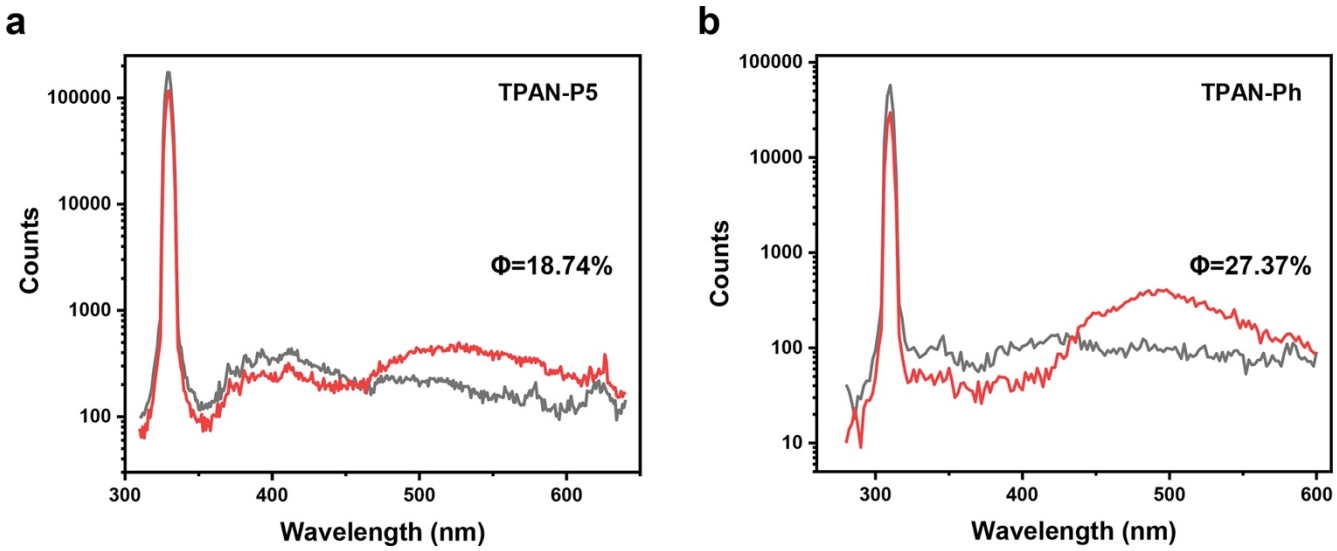

Figure S26. PLQY spectra of TPAN-P5 (a) and TPAN-Ph powders (b).

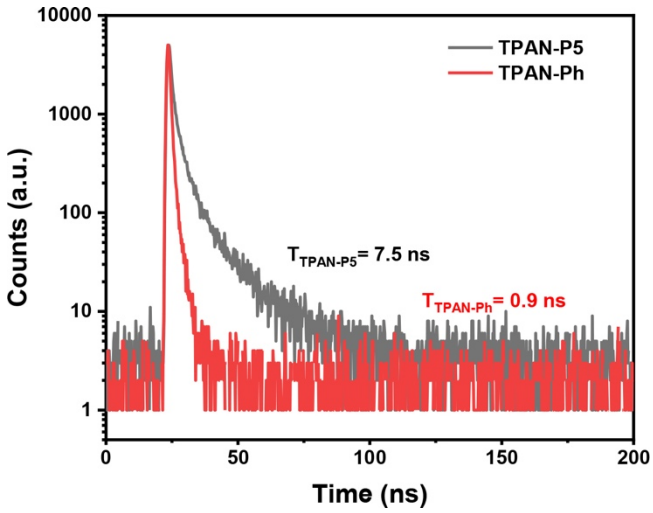

Figure S27. Photoluminescence decay curves for TPAN-P5 (black line) and TPAN-Ph powders (red line).

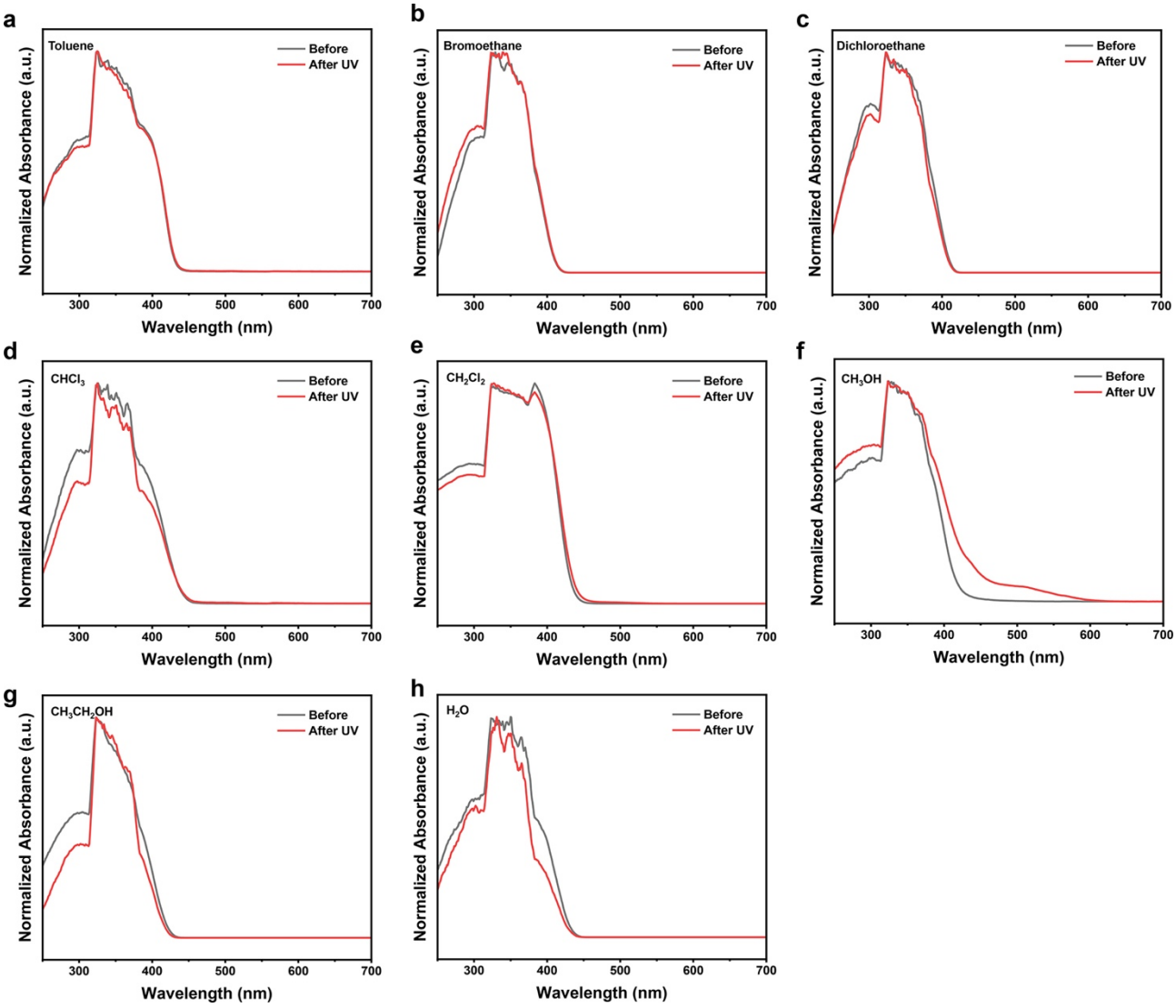

Figure S28. Normalized solid-state UV-Vis absorption spectra of various VOC-fumigated TPAN-P5 powders at the non-irradiated (dark) and UV-irradiated (1 minute UV exposure) states.

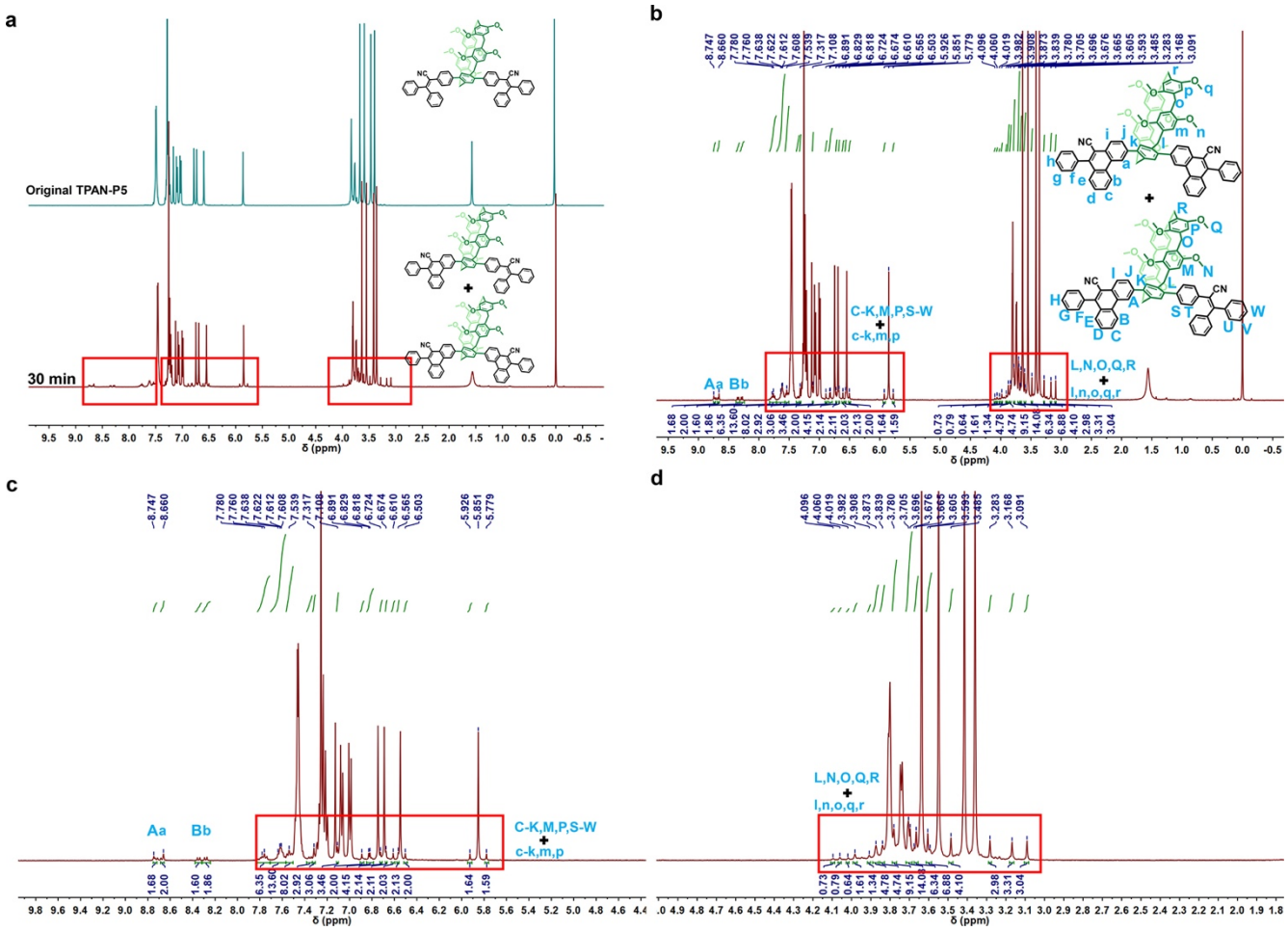

Figure S29. (a) ^{1}H NMR spectra of TPAN-P5-CH_3OH powder before and after UV irradiation (400 MHz, 298 K, $CDCl_3$). (b-d) Full and expanded ^{1}H NMR spectra of the CH_3OH-fumigated TPAN-P5 powder after UV irradiation (400 MHz, 298 K, $CDCl_3$).

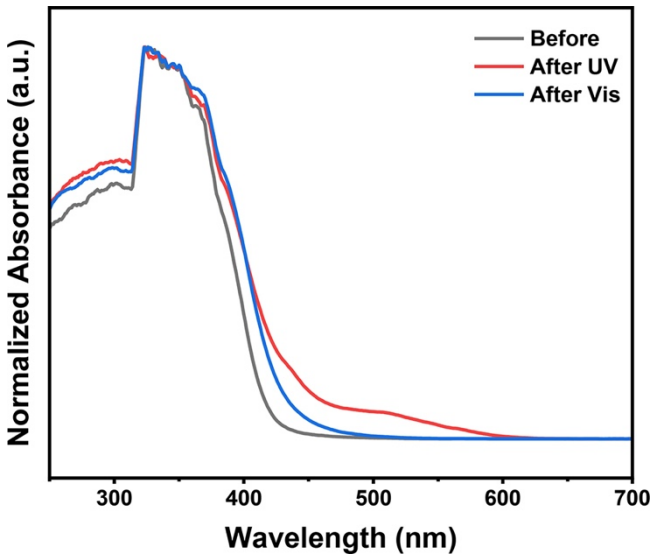

Figure S30. Normalized solid-state UV-Vis absorption spectra of TPAN-P5-CH_3OH powder after different light exposures: initial (black line), UV-irradiated (red line, 1 minute UV exposure), and white light-irradiated for (blue line, 2 minutes white light exposure).

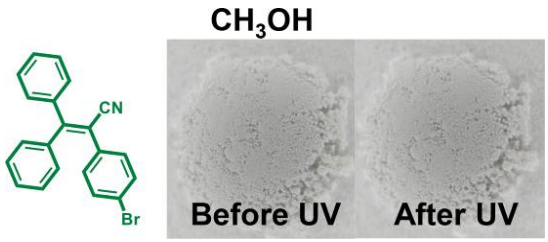

Figure S31. Color photographs of CH_3OH-fumigated TPAN-Br powder before and after UV irradiation for 1 minute.

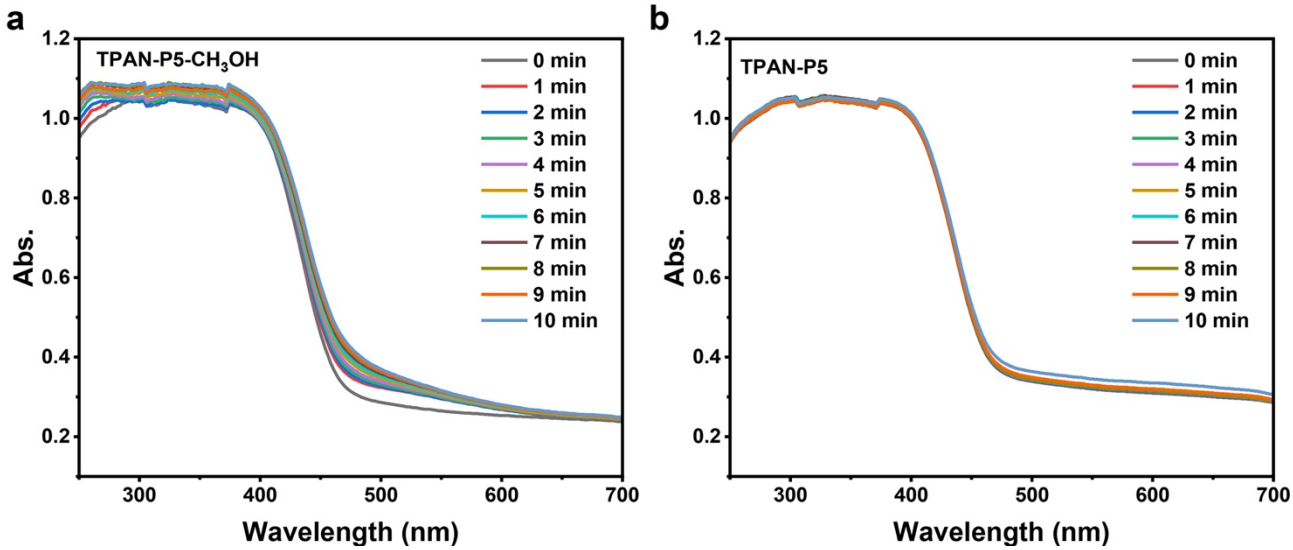

Figure S32. Time-resolved UV-Vis absorption spectra of TPAN-P5-CH_3OH (a) and original TPAN-P5 (b) powders during UV (365 nm) irradiation.

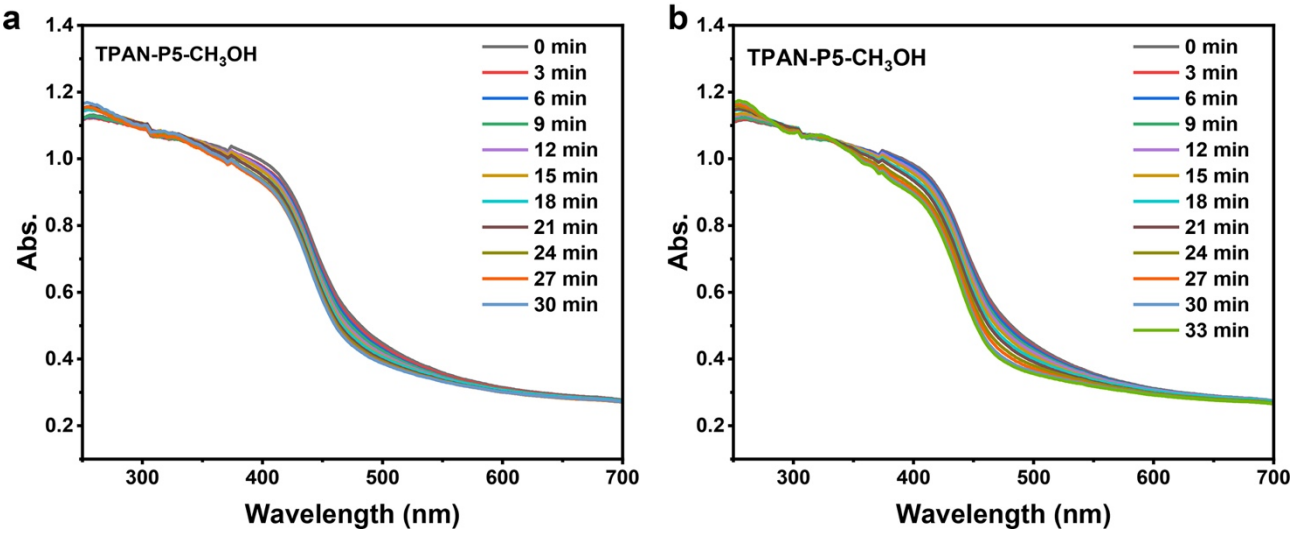

Figure S33. Time-resolved UV-Vis absorption spectra of the TPAN-P5-CH_3OH powder in the dark (a) and during visible light irradiation (b).

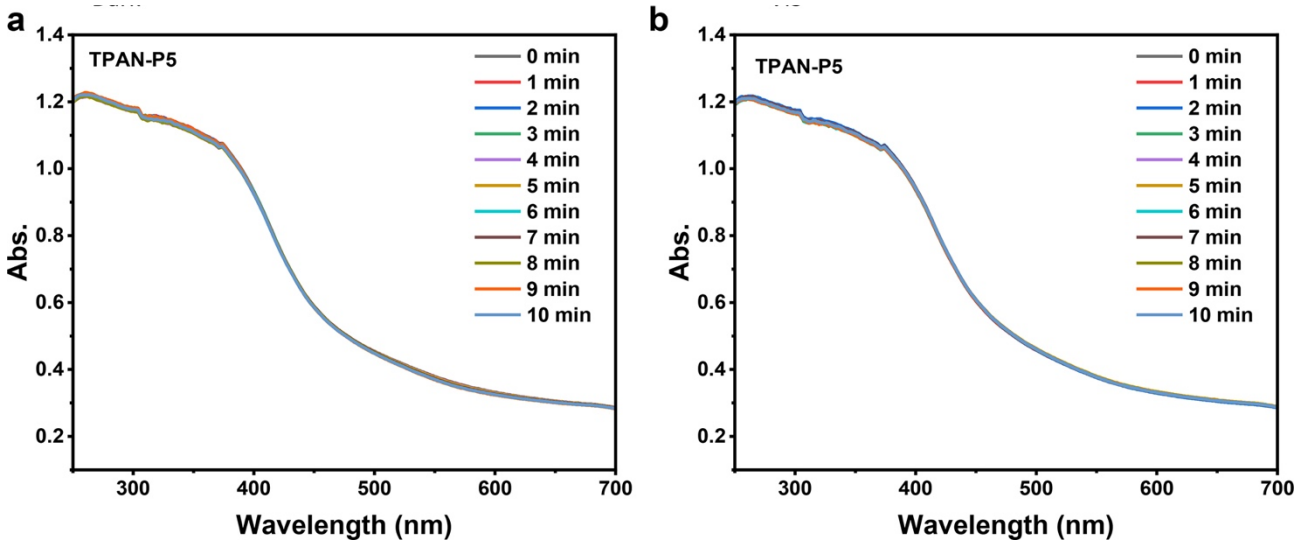

Figure S34. Time-resolved UV-Vis absorption spectra of original TPAN-P5 powder in darkness (a) and under white light (b).

Figure S35. Color photographs of HCOOH-fumigated TPAN-P5 powder before and after UV irradiation for 1 minute.

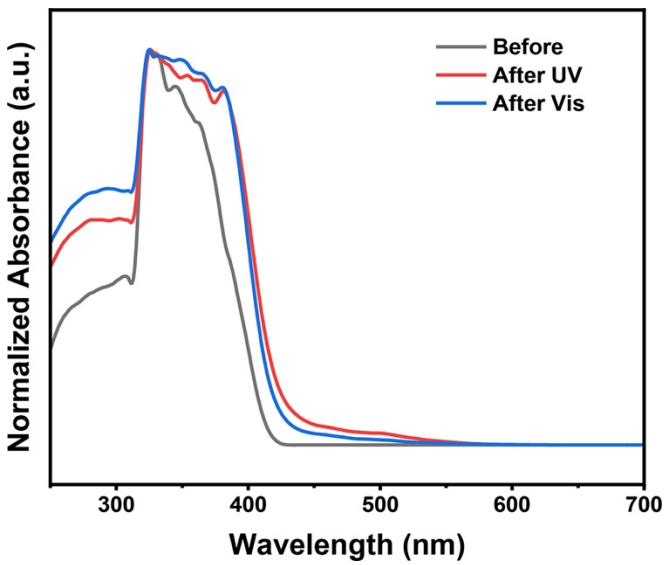

Figure S36. Normalized solid-state UV-Vis absorption spectra of HCOOH-fumigated TPAN-P5 powder after different light exposures: initial (black line), UV-irradiated (red line, 1 minute UV exposure), and white light-irradiated (blue line, 2 minutes white light exposure).

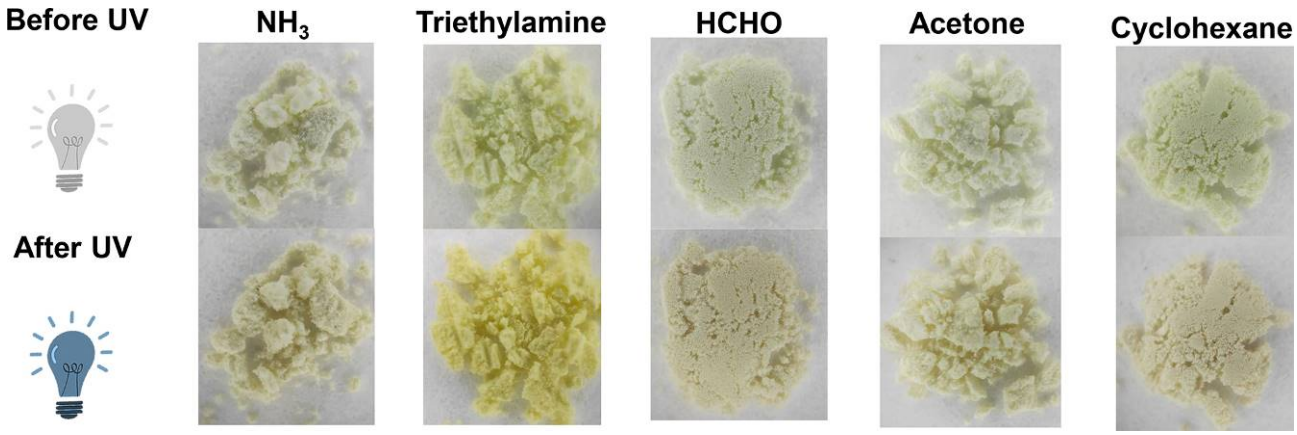

Figure S37. Color photographs of various VOC-fumigated TPAN-P5 powders before and after UV irradiation for 1 minute.

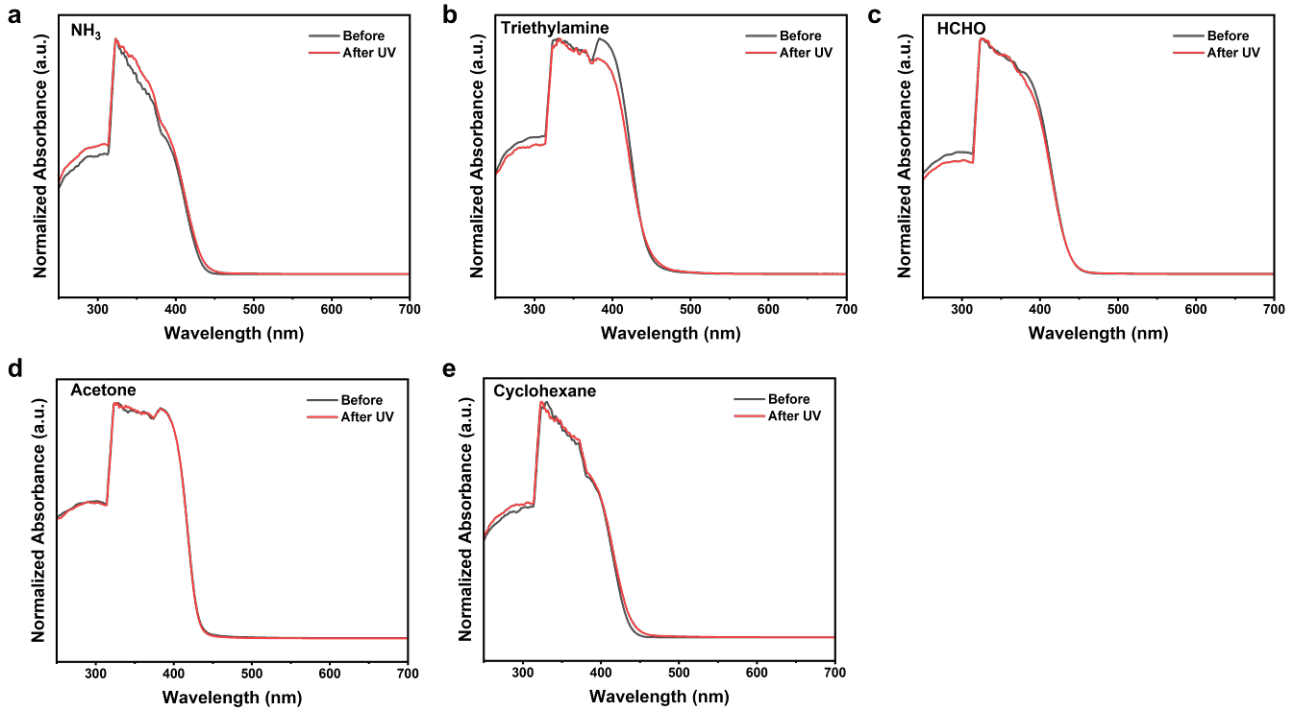

Figure S38. Normalized solid-state UV-Vis absorption spectra of various VOC-fumigated TPAN-P5 powders before and after UV irradiation for 1 minute.

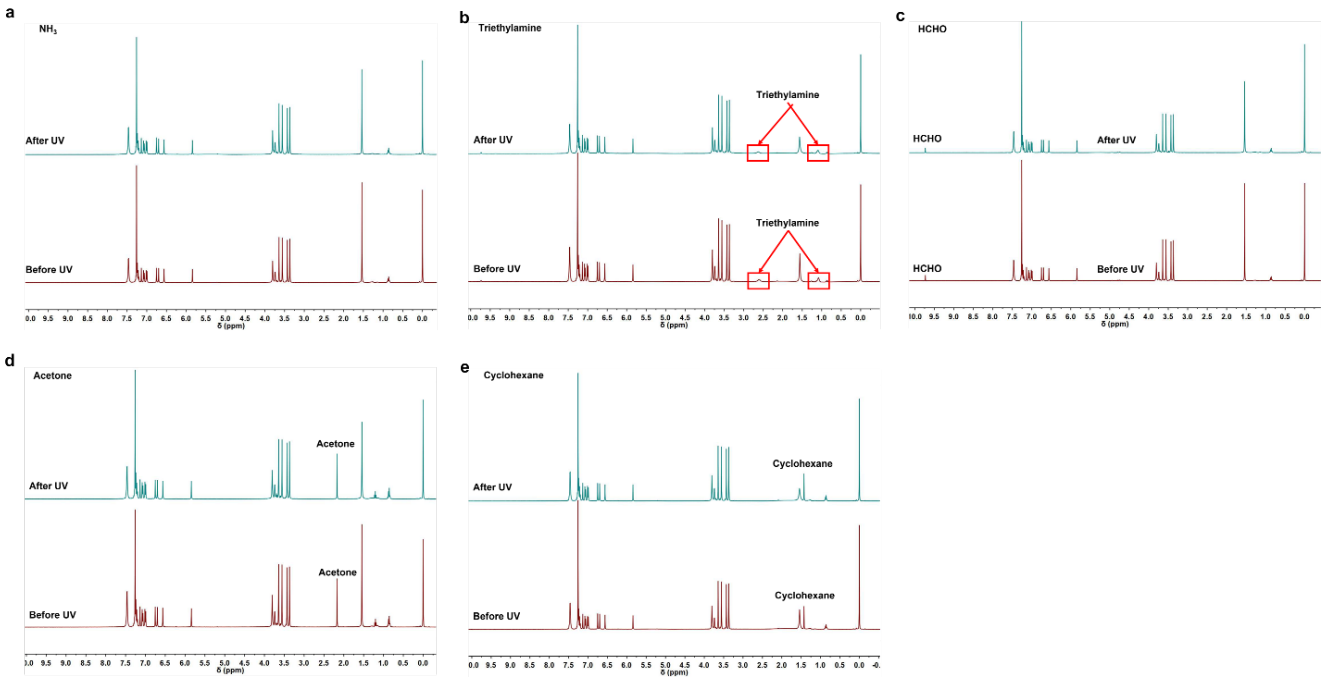

Figure S39. ^{1}H NMR spectra of various VOC-fumigated TPAN-P5 powders before and after UV irradiation for 1 minute (400 MHz, 298 K, $CDCl_3$).

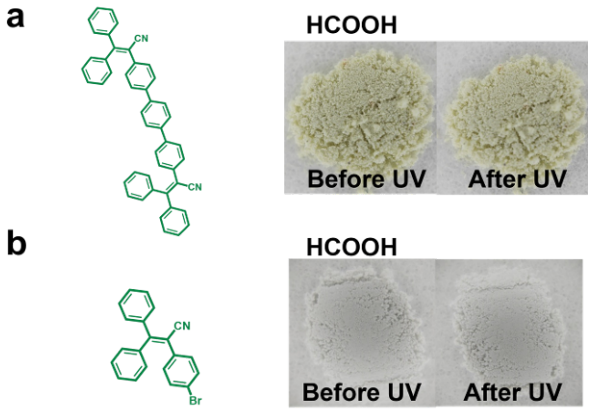

Figure S40. Color photographs of HCOOH-fumigated TPAN-Ph (a) and TPAN-Br (b) powders before and after UV (365 nm) irradiation for 1 minute.

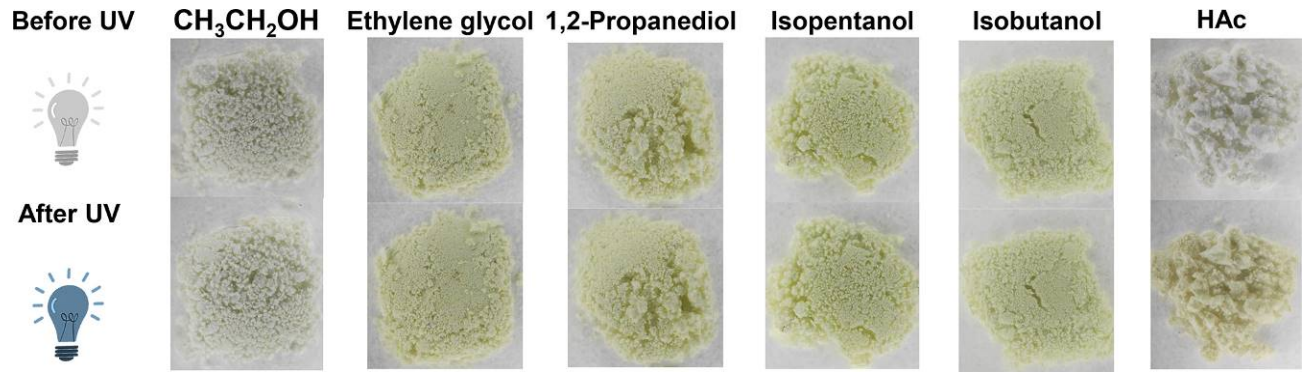

Figure S41. Color photographs of alcohol- and acid-fumigated TPAN-P5 powders before and after UV irradiation for 1 minute.

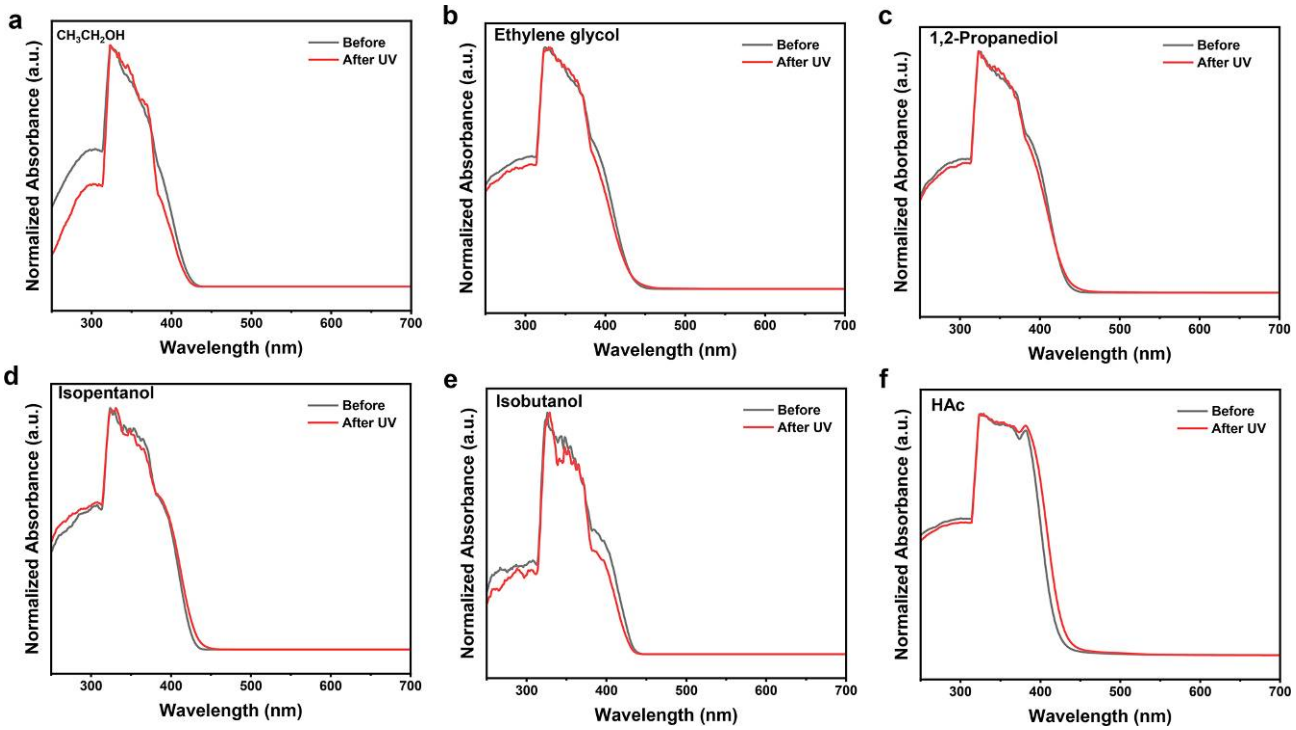

Figure S42. Normalized solid-state UV-Vis absorption spectra of alcohol- and acid-fumigated TPAN-P5 powders before and after UV irradiation for 1 minute.

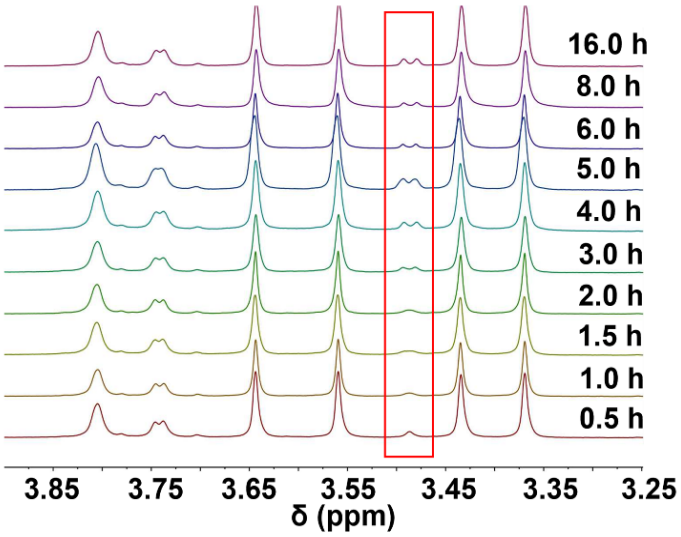

Figure S43. Time-resolved ^{1}H NMR spectra (400 MHz, 298 K, $CDCl_3$) of CH_3OH-fumigated TPAN-P5 powder.

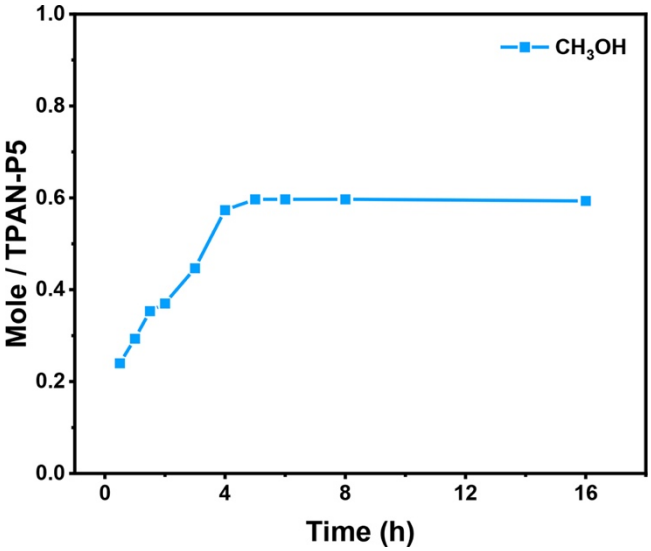

Figure S44. Time-dependent TPAN-P5 solid-vapor adsorption plots for CH_3OH.

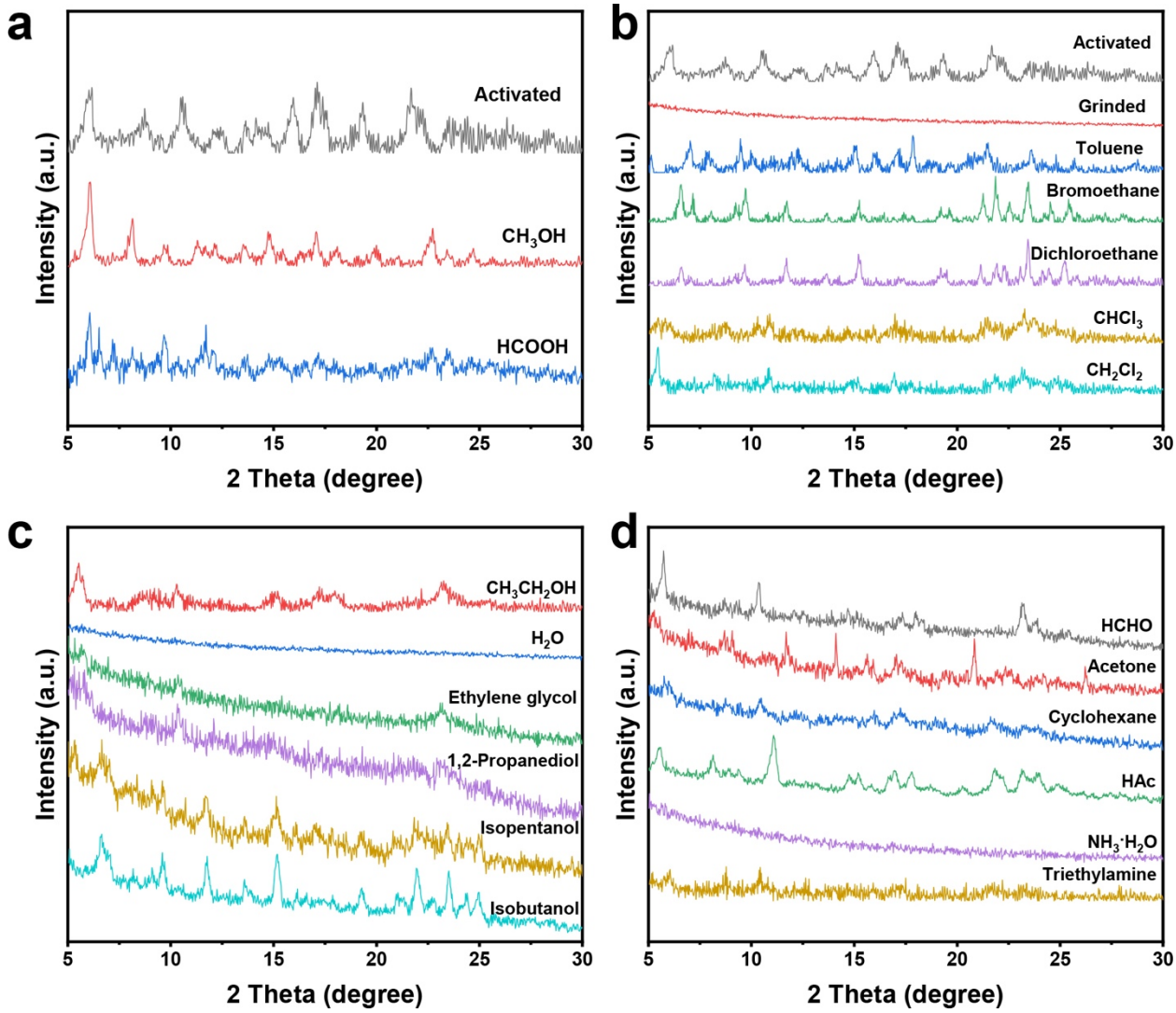

Figure S45. PXRD patterns of various VOC-fumigated TPAN-P5 powders.

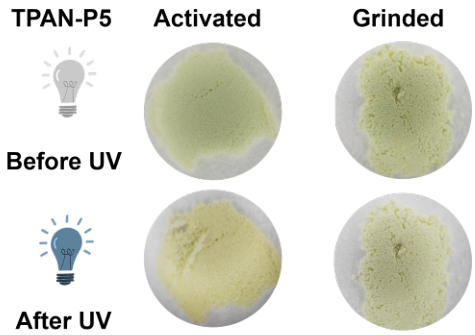

Figure S46. Color photographs of the photochromic properties of TPAN-P5 powder before and after grinding (365 nm UV irradiation for 1 minute).

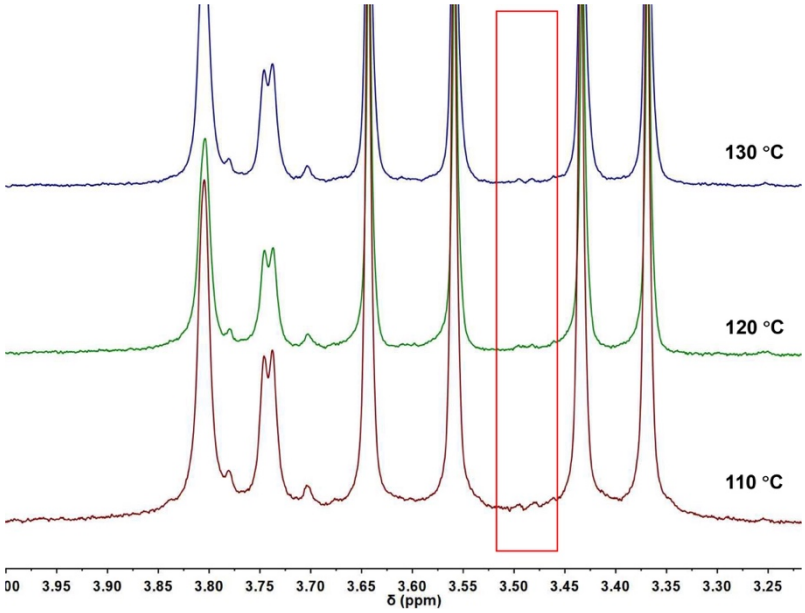

Figure S47. ^{1}H NMR spectra of the TPAN-P5- CH_3OH powder after heating at different temperatures (400 MHz, 298 K, $CDCl_3$).

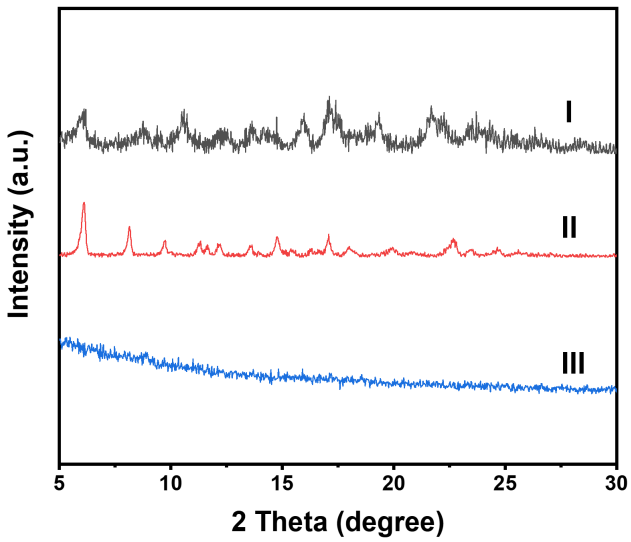

Figure S48. PXRD patterns of TPAN-P5: (I) original TPAN-P5 (black line), (II) after adsorption of CH_3OH vapor (red line), and (III) after heating to remove part of the CH_3OH (blue line).

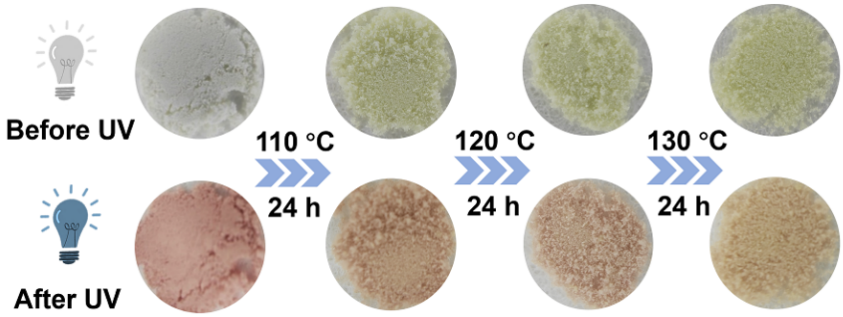

Figure S49. Color photographs of TPAN-P5 powder after partial removal of CH_3OH by heating at different temperatures, both before and after 1 minute of UV irradiation.

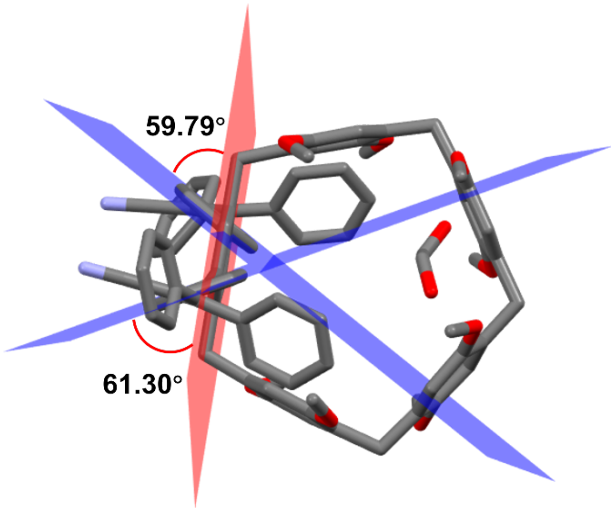

Figure S50. Dihedral angles between terphenyl units in TPAN-P5-CH_3OH. Dihedral angles are measured between the terphenyl units with respect to the pillar[5]arene plane in the TPAN-P5 crystal structure. Hydrogen atoms are omitted for clarity.

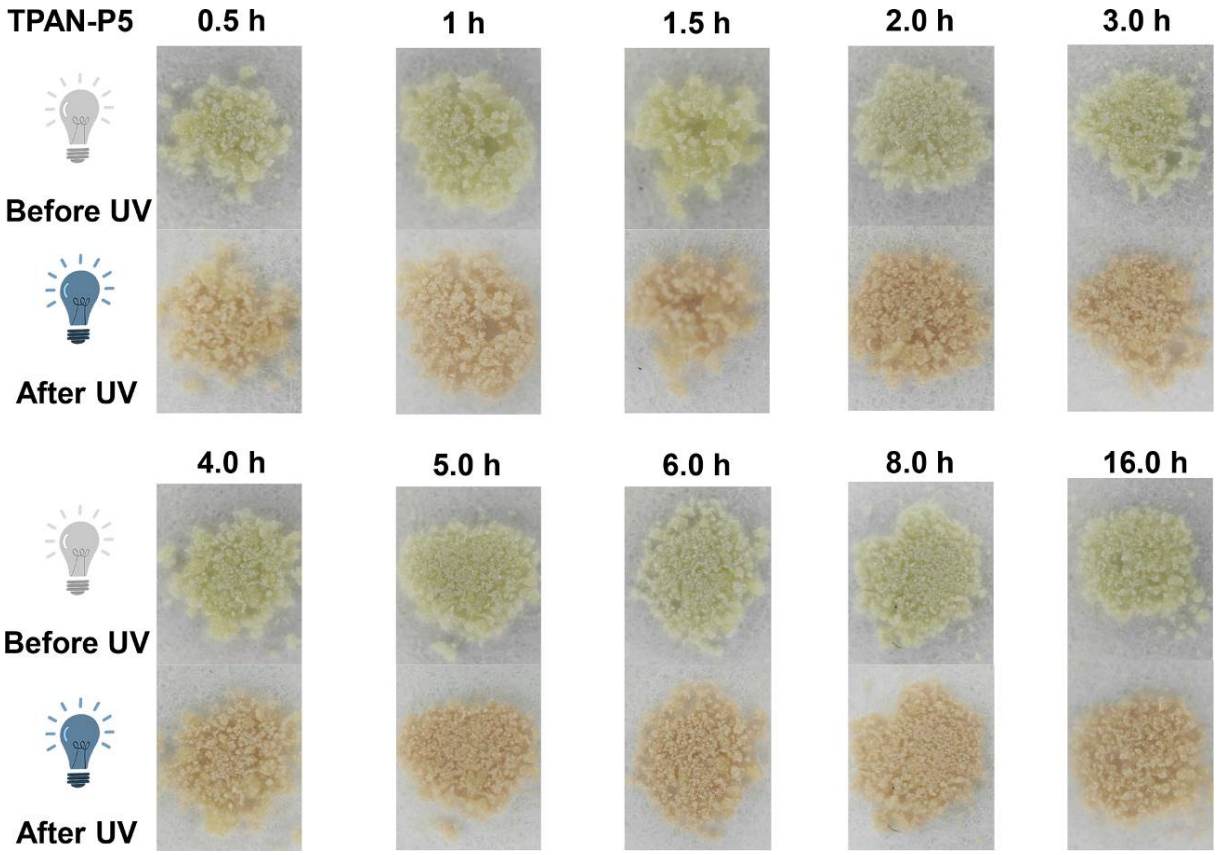

Figure S51. Time-dependent photographs of the TPAN-P5 powder taken before and after UV irradiation after exposure to EA.

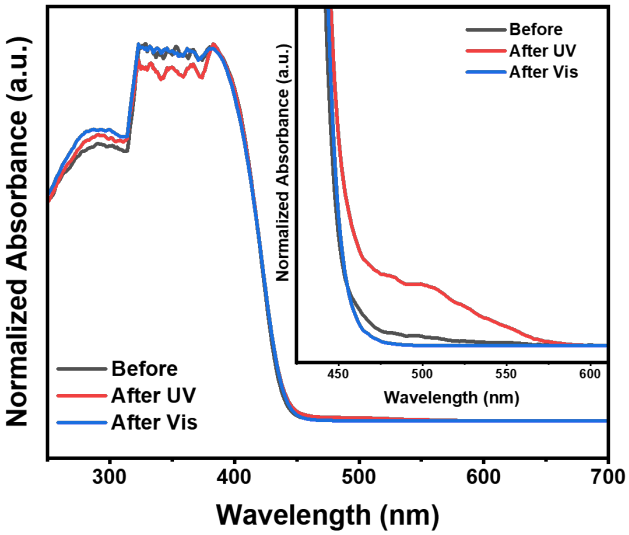

Figure S52. Normalized solid-state UV-Vis absorption spectra of EA-fumigated TPAN-P5 powder after different light exposures: initial (black line), UV-irradiated (red line, 1 minute UV exposure), and white light-irradiated (blue line, 2 minutes white light exposure).

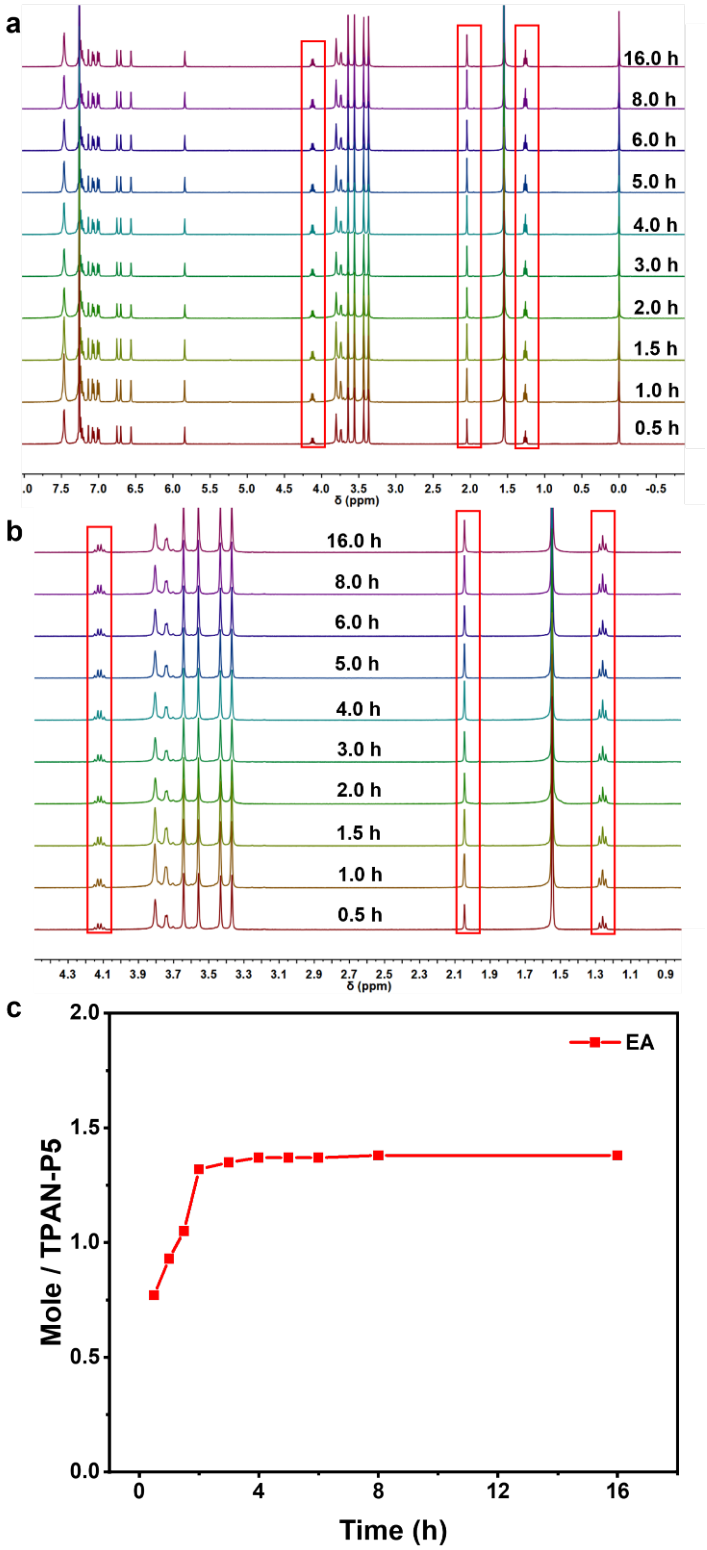

Figure S53. (a and b) Time-resolved ^{1}H NMR spectra (400 MHz, 298 K, $CDCl_3$) of TPAN-P5 after adsorption of EA. (c) Time-dependent TPAN-P5 solid-vapor adsorption plots for EA.

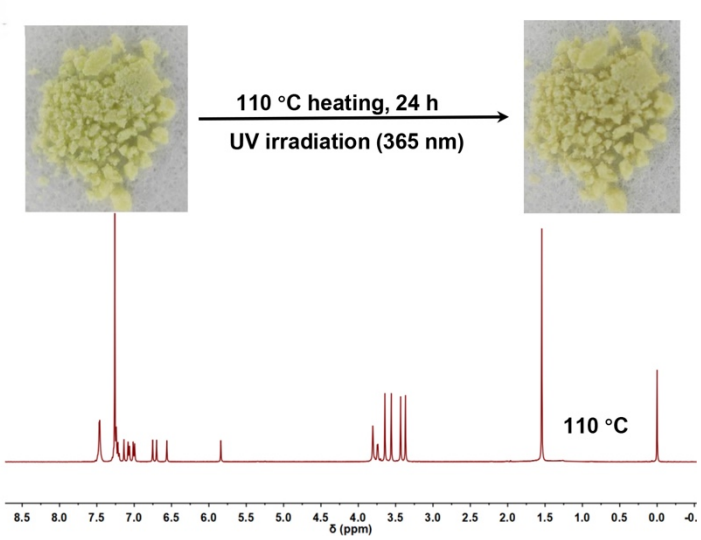

Figure S54. ^{1}H NMR spectrum (400 MHz, 298 K, $CDCl_3$) of EA-fumigated TPAN-P5 powder after heating at 110 °C for 24 hours. Inset: Color photographs of TPAN-P5 powder after EA removal before and after UV irradiation.

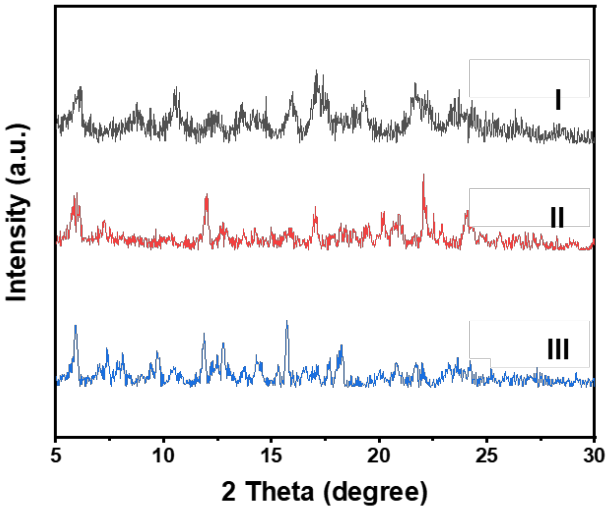

Figure S55. PXRD patterns of TPAN-P5: (I) original TPAN-P5 (black line), (II) after adsorption of EA vapor (red line), and (III) after heating at 110 °C to remove EA from TPAN-P5-EA (blue line).

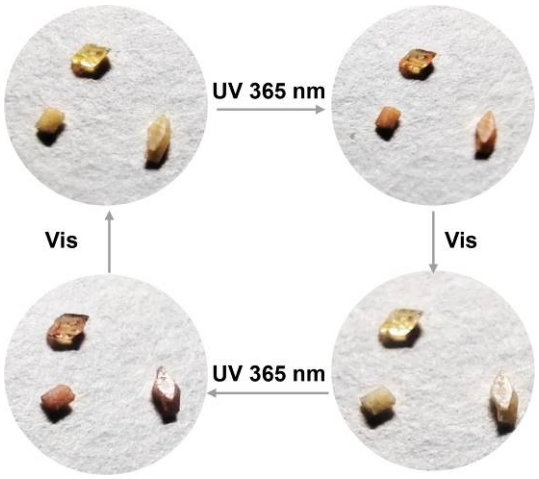

Figure S56. Photochromic cycling process of TPAN-P5-EA crystals.

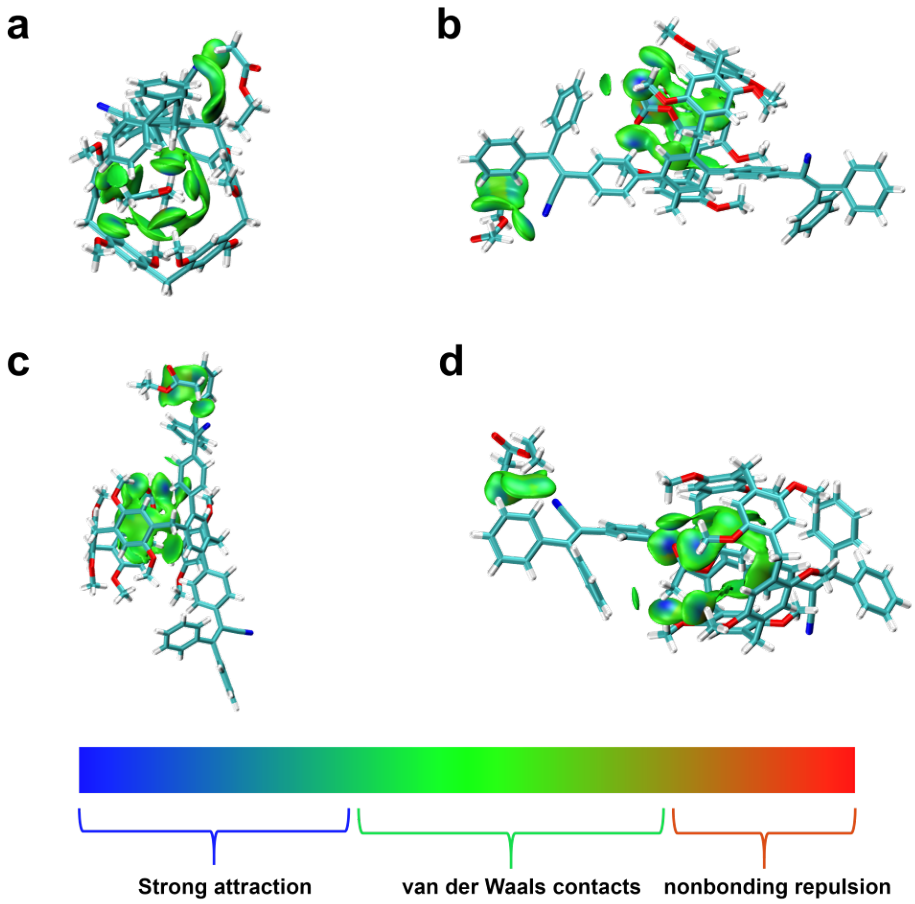

Figure S57. Binding isosurfaces between TPAN-P5 and EA complexes viewed from different angles.

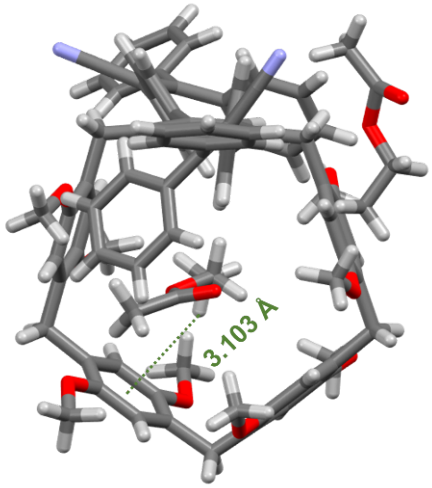

Figure S58. C–H···π (3.103 Å) interaction between TPAN-P5 and EA.

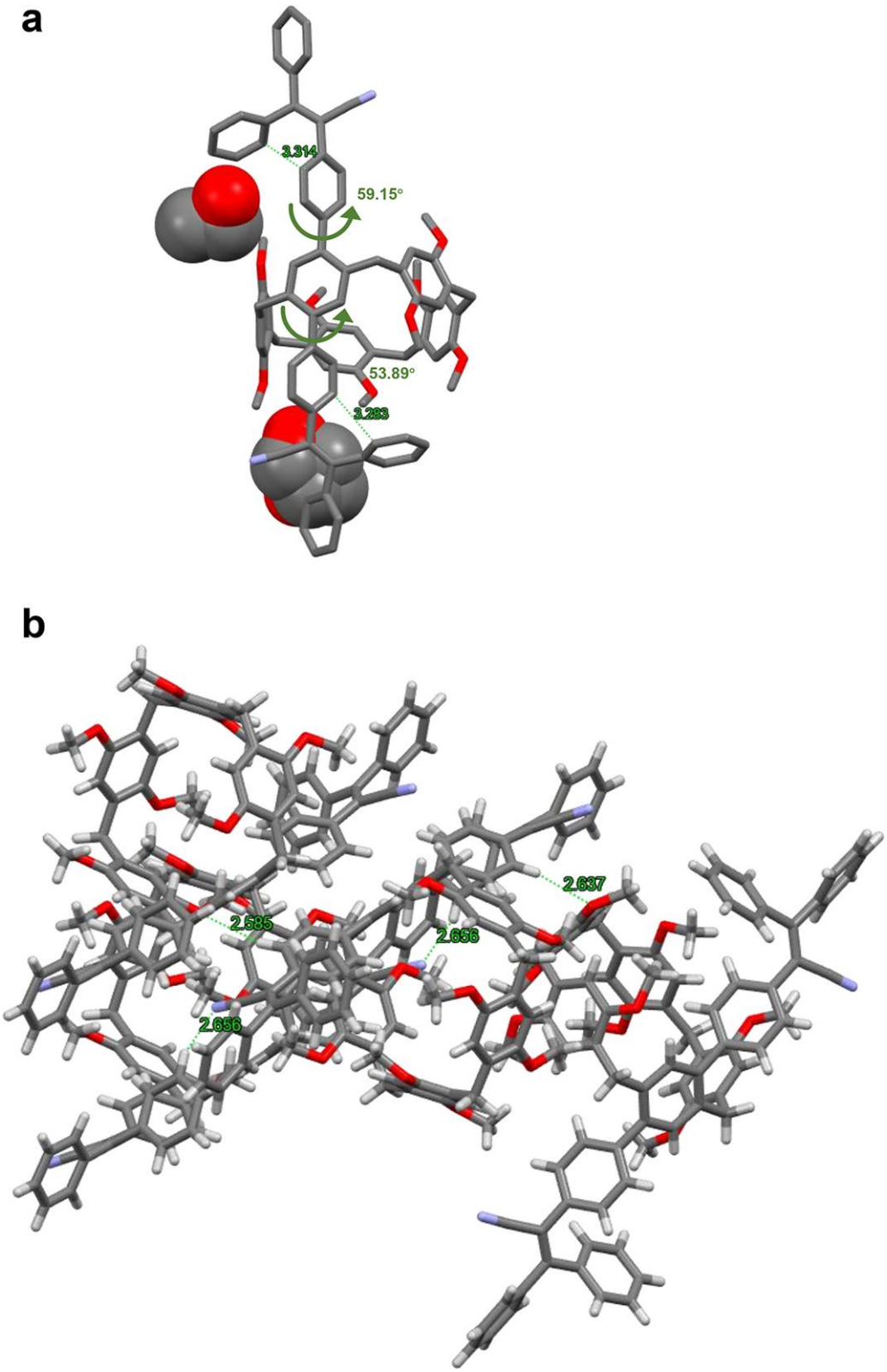

Figure S59. (a) SC-XRD structure of TPAN-P5-CH_3CH_2OH. (b) Intermolecular C–H···O (2.585, 2.637 Å) and C–H···N (2.656 Å) interactions in TPAN-P5-CH_3CH_2OH co-crystal.

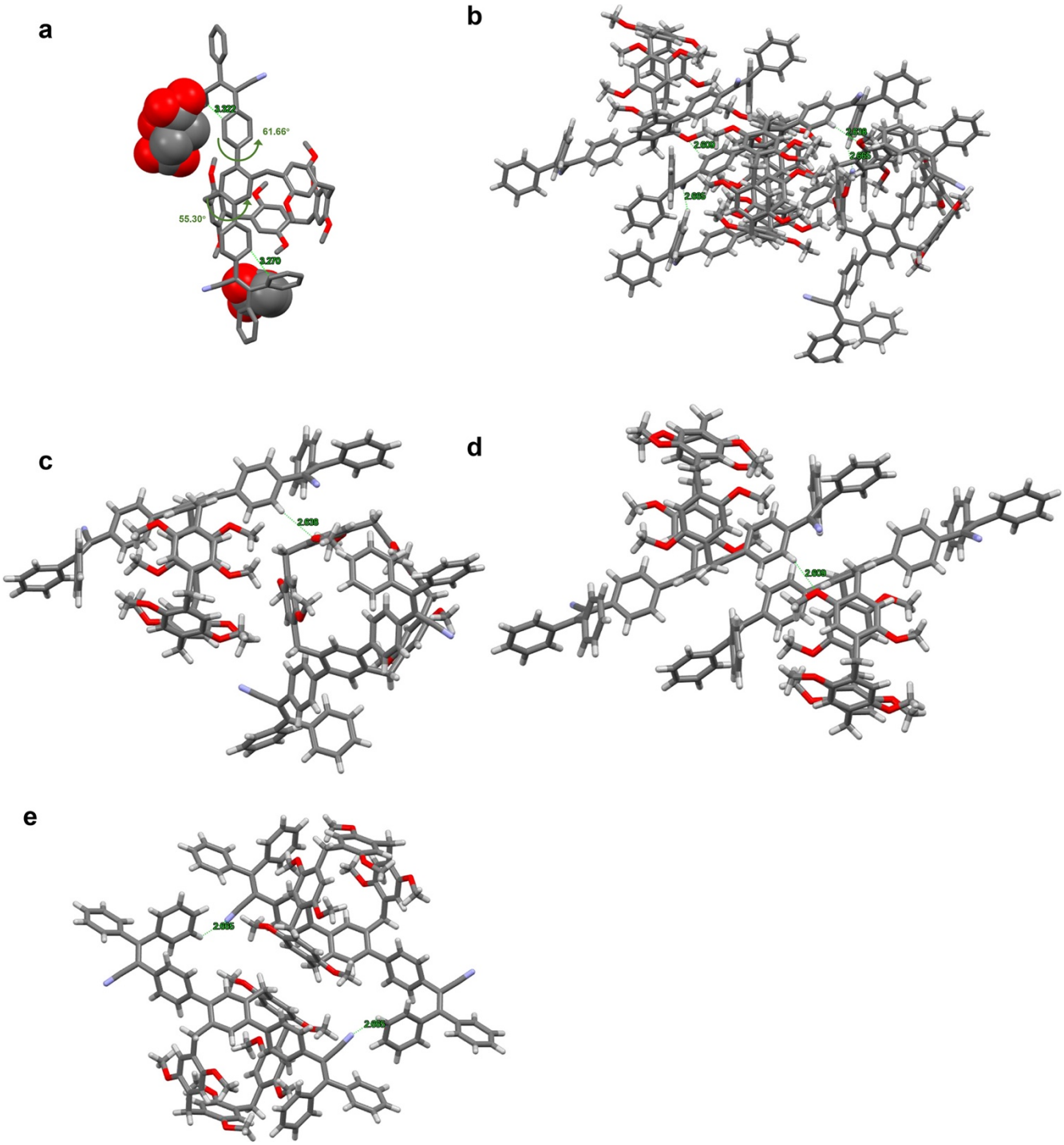

Figure S60. (a) SC-XRD structure of TPAN-P5-CH_3COOH. (b-e) Intermolecular C–H···O (2.638, 2.609 Å) and C–H···N (2.665 Å) interactions in TPAN-P5-CH_3COOH crystal.

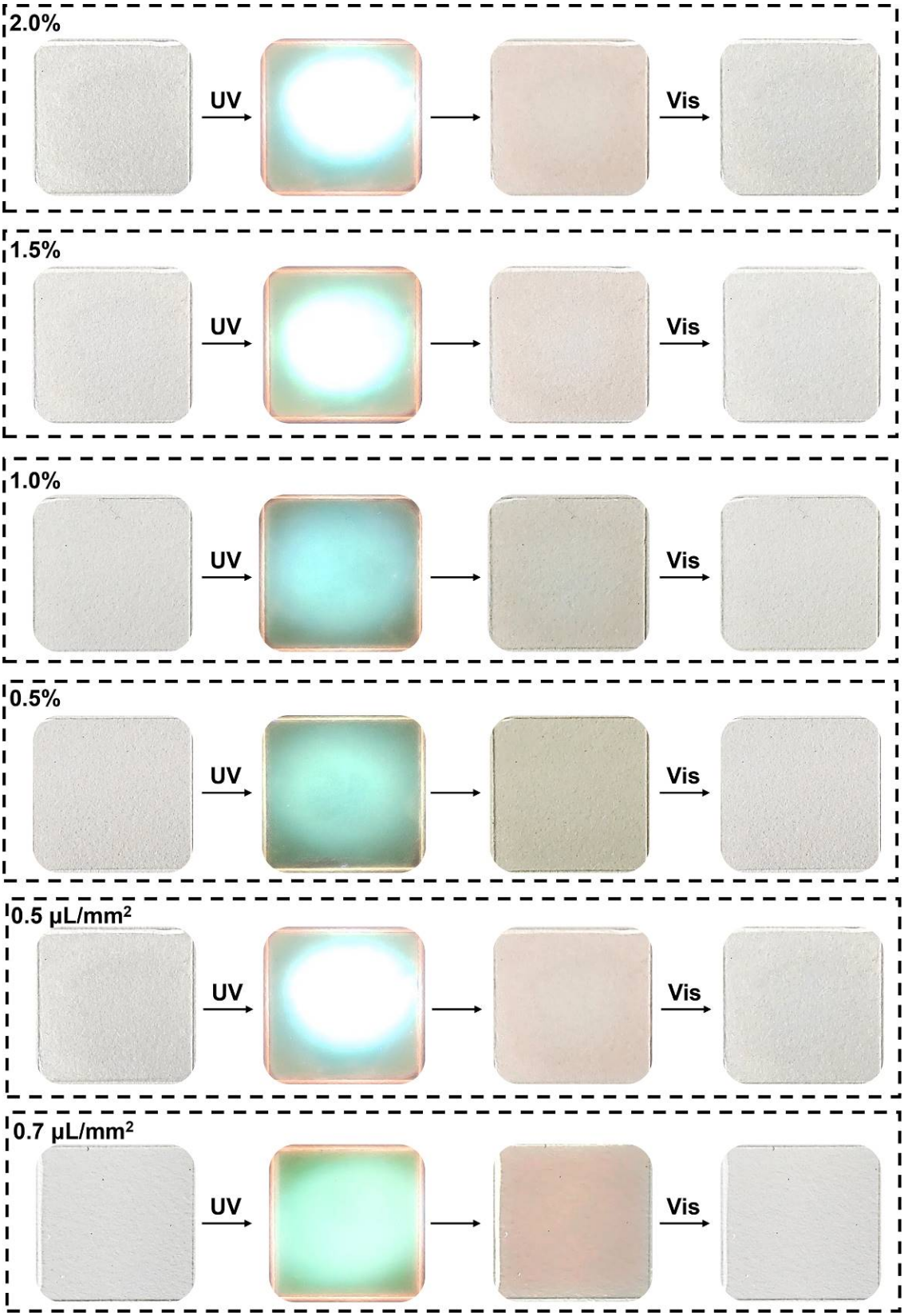

Figure S61. Optimization of preparation conditions and photochromic properties as shown by photographs for TPAN-P5 films.

Section 6. References

S1. C. Lefebvre, G. Rubez, H. Khartabil, J.-C. Boisson, J. Contreras-García and E. Hénon, *Phys. Chem. Chem. Phys.*, 2017, 19, 17928-17936.

S2. T. Lu and F. Chen, *J. Comput. Chem.*, 2012, **33**, 580-592.

S3. W. Humphrey, A. Dalke and K. Schulten, *J. Mol. Graph.*, 1996, **14**, 33-38.

S4. M. J. Frisch, G. W. Trucks, H. B. Schlegel, G. E. Scuseria, M. A. Robb, J. R. Cheeseman, G. Scalmani, V. Barone, G. A. Petersson, H. Nakatsuji, X. Li, M. Caricato, A. V. Marenich, J. Bloino, B. G. Janesko, R. Gomperts, B. Mennucci, H. P. Hratchian, J. V. Ortiz, A. F. Izmaylov, J. L. Sonnenberg, Williams, F. Ding, F. Lipparini, F. Egidi, J. Goings, B. Peng, A. Petrone, T. Henderson, D. Ranasinghe, V. G. Zakrzewski, J. Gao, N. Rega, G. Zheng, W. Liang, M. Hada, M. Ehara, K. Toyota, R. Fukuda, J. Hasegawa, M. Ishida, T. Nakajima, Y. Honda, O. Kitao, H. Nakai, T. Vreven, K. Throssell, J. A. Montgomery Jr., J. E. Peralta, F. Ogliaro, M. J. Bearpark, J. J. Heyd, E. N. Brothers, K. N. Kudin, V. N. Staroverov, T. A. Keith, R. Kobayashi, J. Normand, K. Raghavachari, A. P. Rendell, J. C. Burant, S. S. Iyengar, J. Tomasi, M. Cossi, J. M. Millam, M. Klene, C. Adamo, R. Cammi, J. W. Ochterski, R. L. Martin, K. Morokuma, O. Farkas, J. B. Foresman and D. J. Fox, Gaussian 16 Rev. C.01.*Journal*, 2016.

S5. Q. Li, Y. Wu, J. Cao, Y. Liu, Z. Wang, H. Zhu, H. Zhang and F. Huang, *Angew. Chem. Int. Ed.*, 2022, **61**, e202202381.

S6. Z. Li, X. Li and Y.-W. Yang, *Small*, 2019, **15**, 1805509.